DOI: https://doi.org/10.15407/pmach2026.03.017

UDC 532.51:537.84:532.135

ELECTRICALLY CONDUCTING MHD CASSON NANOFLUID FLOW IN A UNIFORM TRANSVERSE MAGNETIC FIELD OVER A STRETCHING SHEET

[1] Felix T. Onojovwo
ORCID: 0009-0002-1293-7434

[2] Anselm O. Oyem
oanselmoyem.sci@busitema.ac.ug
ORCID: 0000-0002-1756-0333

[1] Sunday O. Imoni
ORCID: 0009-0000-2664-841X

[1] Jessica M. Gyegwe
ORCID: 0000-0002-2082-1063

[1] Federal University Lokoja
P. M. B. 1154, Lokoja, Nigeria

[2] Busitema University
P.O. Box 236, Tororo, Uganda

This study focuses on volumetric sensible enthalpy formulation of ethylene glycol-based nanofluids that replaces the conventional temperature-based energy equation. The nanofluid contains Al_2O_3 nanoparticles with volume fractions in the range ($0.01 \leq \varphi \leq 0.05$), consistent with experimentally investigated concentrations. Unlike conventional temperature-based energy formulations, the present approach describes thermal transport through volumetric sensible enthalpy, representing the sensible energy stored per unit volume of the nanofluid. This framework enables the analysis of coupled momentum, enthalpy, and nanoparticle transport in electrically conducting Casson nanofluids involving thermophoresis, viscous dissipation, and Joule heating. The governing momentum, enthalpy, and nanoparticle concentration equations were transformed into coupled nonlinear ordinary differential equations using similarity transformations and solved numerically using an adaptive collocation scheme (SciPy's solve_bvp). Parameter effects are systematically evaluated, including the Casson parameter, magnetic field parameter, Schmidt number, Biot number, thermal and solute Grashof numbers, Brinkman number, Eckert number and thermophoresis parameter. The results show that the magnetic field parameter and Casson rheological effects strongly influence the momentum characteristics of the flow. Increasing the magnetic field parameter suppresses the velocity distribution through the Lorentz force while enhancing the volumetric sensible enthalpy due to Joule heating. The Eckert number produces a significant increase in volumetric sensible enthalpy owing to viscous dissipation, whereas the Schmidt number primarily controls nanoparticle concentration transport with only a weak influence on the enthalpy field. Thermal and solutal buoyancy parameters enhance fluid motion through buoyancy-driven convection, while thermophoresis promotes nanoparticle migration and moderately increases thermal energy storage within the boundary layer. In contrast, the Biot and Brinkman numbers exhibit limited influence on the velocity, volumetric sensible enthalpy, and concentration profiles within the considered parameter ranges. The proposed volumetric sensible enthalpy formulation provides an alternative framework for quantifying internal energy storage and redistribution in MHD non-Newtonian nanofluids. Potential applications include thermal energy storage, electronic cooling with nanofluids, polymer extrusion, magnetohydrodynamics (MHD) pumping, biomedical flows, solar thermal collection, and nuclear reactor cooling.

***Keywords**: volumetric sensible enthalpy, enthalpy formulation, mixed convection, MHD, Brinkman number, nanoparticle transport.*

Introduction

Nanofluids have attracted considerable attention in recent years owing to their enhanced thermal transport capabilities and wide applicability in modern engineering systems such as microelectronic cooling, solar thermal collectors, nuclear reactors, biomedical devices, and industrial heat exchangers [1]. Nanofluids are engineered by dispersing nanoparticles, such as metallic or metal-oxide particles, into conventional base fluids to improve their thermal conductivity and heat transfer performance [2]. Among the various nanoparticles employed in thermal systems, aluminum oxide (Al_2O_3) nanoparticles (range $0.01 \leq \varphi \leq 0.05$), dispersed in ethylene glycol at different volume fractions have demonstrated excellent thermal stability and enhanced convective heat transfer characteristics [3]. The enhancement in thermal and transport properties strongly depends on the nanoparticle concentration and dispersion characteristics. The practical relevance of Al_2O_3–ethylene glycol nanofluids has been demonstrated through several experimental investigations. Experimental studies have shown that the thermophysical properties of Al_2O_3–based ethylene glycol and ethylene glycol–water nanofluids

This paper is licensed under a Creative Commons Attribution 4.0 International License.
© Felix T. Onojovwo, Anselm O. Oyem, Sunday O. Imoni, Jessica M. Gyegwe, 2026

depend strongly on nanoparticle concentration, temperature, and suspension characteristics. In particular, increasing the nanoparticle volume fraction generally enhances the effective thermal conductivity and heat transfer capability, although it also increases the effective viscosity and hydraulic resistance [4–7]. These experimentally established trends have motivated the application of Al_2O_3–based nanofluids in electronic cooling systems, compact heat exchangers, automotive cooling, and solar thermal energy systems, where efficient heat removal is essential. Furthermore, when these electrically conducting nanofluids are subjected to a uniform transverse magnetic field, magnetohydrodynamic (MHD) control provides an additional mechanism for regulating fluid motion and heat transfer, making them attractive for advanced thermal management and energy conversion technologies. Such MHD-controlled nanofluid flows are also relevant to liquid metal cooling in nuclear reactors, electromagnetic casting, and plasma processing applications. Consequently, mathematical models that accurately describe the coupled momentum, thermal, and nanoparticle transport behaviour of MHD Al_2O_3–ethylene glycol nanofluids are of considerable practical importance.

The study of magnetohydrodynamic (MHD) nanofluid flow has gained significant attention because electrically conducting fluids are widely encountered under magnetic fields in metallurgical processing, magnetic drug targeting, electronic cooling, petroleum engineering, crystal growth, and energy conversion [8, 9]. An external magnetic field generates Lorentz forces that considerably alter the fluid momentum and heat transfer [10]. In many practical thermal systems, working fluids with higher nanoparticle concentrations ranging from φ=1% to 5% in this study exhibits non-Newtonian rather than ideal Newtonian behaviour due to enhanced particle interactions and concentration-dependent effects. Therefore, non-Newtonian models such as the Casson formulation are employed to represent the rheological behaviour of such fluids. Among non-Newtonian models, the Casson fluid model has been extensively adopted owing to its ability to describe yield-stress materials such as blood, polymer suspensions, printing inks, molten chocolate, and honey [11, 12]. Consequently, MHD Casson nanofluid flow analysis has emerged as an active research area in transport phenomena, with recent investigations focusing on thermal radiation, Joule heating, porous media, activation energy, and hybrid nanofluid applications [13–15].

In boundary layer transport, mechanisms such as thermophoresis, Brownian motion, viscous dissipation, thermal radiation, and chemical reactions considerably alter the thermal and concentration distributions [16]. Thermophoresis drives nanoparticle migration from hotter to cooler regions under temperature gradients, thereby modifying the concentration and energy transport. Brownian motion accounts for random nanoparticle movement, contributing significantly to thermal diffusion. Viscous dissipation converts kinetic energy into internal thermal energy owing to frictional heating, particularly in high-speed or highly viscous flows. Among the dimensionless parameters characterizing viscous dissipation, the Eckert number (Ec) represents the conversion of kinetic energy into internal energy, whereas the Brinkman number (Br) measures viscous dissipation relative to conductive heat transfer. These coupled mechanisms strongly influence heat and mass transfer in nanofluid systems under various flow configurations, including flows over stretching surfaces, channels, and other thermal engineering devices [17–19]. Among these configurations, stretching surfaces have received considerable attention because of their relevance to polymer processing, coating, extrusion, and cooling applications.

Stretching surface flow problems arise in various industrial processes, including polymer extrusion, wire drawing, metal spinning, and continuous casting [20, 21]. In such applications, the incorporation of nanofluids can enhance thermal transport performance, while product quality depends strongly on the thermal and concentration distributions within the boundary layer. Therefore, accurate mathematical modeling of heat and mass transport over stretching surfaces remains an important research topic. Most previous investigations of nanofluid flow have formulated the thermal transport equation using temperature as the primary energy variable, while incorporating nanoparticle-dependent thermophysical properties such as thermal conductivity, heat capacity, and viscosity. Although this temperature-based formulation has been widely applied, it may not explicitly represent the volumetric sensible enthalpy associated with energy storage and dissipation effects. Therefore, the present study adopts an enthalpy-based formulation to provide an alternative description of coupled momentum, thermal, and nanoparticle transport. Recent studies have shown that MHD nanofluid transport over stretching sheets has been investigated under diverse physical effects, including chemical reactions, thermal radiation, viscous dissipation, and bioconvection [22–32]. Most of these studies adopted temperature-based energy equations while differing mainly in the constitutive fluid model and additional transport mechanisms. However, none reformulated the energy equation using volumetric sensible en-

thalpy as the primary thermal variable. Consequently, the direct representation of internal energy storage and redistribution in electrically conducting Casson nanofluids remains largely unexplored.

However, temperature alone does not fully capture the thermal energy storage characteristics of nanofluids, particularly in systems involving viscous heating and nanoparticle interactions. To overcome this limitation, the present study adopts a volumetric sensible enthalpy formulation that directly accounts for the internal energy content rather than temperature variations. This formulation is particularly suitable for advanced thermal systems involving coupled thermofluidic interactions, energy storage and redistribution. While most existing enthalpy-based studies have primarily focused on phase change and latent heat applications, the application of the sensible enthalpy framework to MHD Casson nanofluid flow with thermophoresis and viscous dissipation remains largely unexplored. For example, [33] developed an enthalpy-based lattice Boltzmann method for solid–liquid phase-change heat transfer in metal foams under local thermal non-equilibrium conditions, using enthalpy as the primary thermal variable. [34] proposed a low-Mach-number enthalpy method for non-isothermal gas–liquid–solid flows involving melting and solidification, incorporating density variations and phase-transition effects. Similarly, [35] presented a generalized energy equation with enthalpy diffusion for multicomponent droplet heat and mass transfer, demonstrating the importance of sensible enthalpy transport in accurately describing the evaporation processes. These studies establish the thermodynamic relevance of enthalpy formulations; however, their application to electrically conducting non-Newtonian nanofluid boundary layer flow with simultaneous magnetic effects, thermophoresis, and viscous dissipation has not yet been adequately investigated.

The study investigates an enthalpy-based formulation for MHD Casson nanofluid flow over a stretching sheet, accounting for coupled momentum and thermal transport phenomena, including thermophoresis, viscous and thermal dissipation, and Joule heating. The governing PDEs for momentum, sensible enthalpy, and nanoparticle concentration were transformed into coupled ODEs via similarity transformations. Numerical solutions examine the effects of key parameters: Casson parameter, magnetic parameter, Brownian motions, thermophoresis parameter, Schmidt number, Biot number, thermal and solutal Grashof numbers, Brinkman number, and Eckert number on velocity, sensible enthalpy, and concentration profiles. Despite these contributions, most existing studies on MHD Casson nanofluid boundary-layer flow formulate thermal transport using temperature as the primary variable, restricting the analysis to wall temperature distributions and external thermal boundary-layer characteristics. In contrast, this study introduces an enthalpy transport model in which the energy equation is recast in terms of internal energy density rather than temperature. The key novel aspects of this study are as follows:

(i) The application of a volumetric sensible enthalpy formulation to the MHD Casson nanofluid flow over a stretching surface, which has not been previously reported in the literature.

(ii) The simultaneous incorporation of thermophoretic particle migration and viscous dissipation (via both Eckert and Brinkman numbers) within the enthalpy framework, enabling direct tracking of internal energy storage and redistribution.

(iii) The use of a volumetric sensible enthalpy formulation that explicitly accounts for the coupled effects of Lorentz force, Joule heating, thermophoresis, Brownian motion, and dual buoyancy forces on energy transport.

(iv) A systematic parametric evaluation of the Casson parameter, magnetic parameter, Schmidt number, Biot number, thermal and solutal Grashof numbers, Eckert number, Brinkman number, and thermophoresis parameter on velocity, volumetric sensible enthalpy, and concentration fields.

Unlike conventional temperature-based models that focus on wall heat flux, the volumetric sensible enthalpy formulation provides a thermodynamic framework for analyzing the internal energy pathways in electrically conducting non-Newtonian nanofluids. This approach establishes a foundation for extending enthalpy-based analyses to more complex scenarios involving property variations, phase changes, or large temperature ranges.

Mathematical Formulation of the Problem

This study examines the steady two-dimensional boundary layer transport of an electrically conducting Casson nanofluid over a stretching surface. The sheet is stretched at a velocity $U(x) = ax$, where, a>0 is the constant stretching rate. A uniform transverse magnetic field of strength B_0 is applied perpendicular to the sheets. The nanofluid consisted of aluminum oxide (Al_2O_3) nanoparticles suspended in ethylene glycol as the base fluid. The physical configuration incorporates nanoparticle transport effects, thermophoretic particle migration, viscous dissipation, Joule heating, and buoyancy forces arising from thermal and concentration gradients. Unlike

conventional temperature-based formulations, this study employs a volumetric sensible enthalpy framework in which the thermal energy transport is expressed in terms of the internal energy density as follows:

$$\hat{h} = \rho_{nf} c_{p,nf} (T - T_\infty),$$

where $\hat{h}$ represents the internal energy content per unit volume relative to the ambient state; ρ_{nf} is the nanofluid density; c_{nf} is its specific heat at constant pressure; T is the local temperature, and T_∞ is the ambient temperature (Fig. 1). This formulation directly tracks the volumetric energy storage and redistribution within the nanofluid boundary layer.

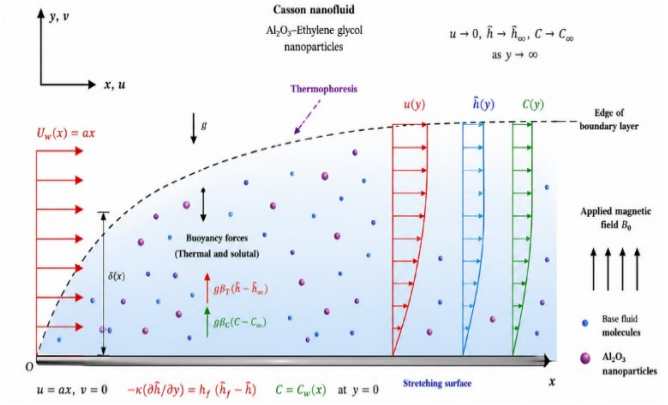


Fig. 1. Schematic diagram of the flow

Under the usual boundary layer and the Boussinesq approximations for buoyancy, the governing conservation equations for mass, momentum, volumetric sensible enthalpy, and nanoparticle concentration are

$$\frac{\partial u}{\partial x} + \frac{\partial v}{\partial y} = 0; \tag{1}$$

$$u\frac{\partial u}{\partial x} + v\frac{\partial v}{\partial y} = \frac{\mu_{nf}}{\rho_{nf}}\left(1 + \frac{1}{\beta}\right)\frac{\partial^2 u}{\partial y^2} + g\beta_T\left(\frac{\hat{h}}{\rho_{nf} c_{pnf}}\right) + g\beta_c (C - C_\infty) - \frac{\sigma_{nf} B_0^2 u}{\rho_{nf}}; \tag{2}$$

$$u\frac{\partial \hat{h}}{\partial x} + v\frac{\partial \hat{h}}{\partial y} = \frac{\partial}{\partial y}\left(\frac{\kappa(\hat{h})}{\rho_{nf} c_{pnf}}\frac{\partial \hat{h}}{\partial y}\right) + \tau\frac{D_T}{T_\infty}\frac{1}{(\rho_{nf} c_{pnf})^2}\left(\frac{\partial \hat{h}}{\partial y}\right)^2 + \frac{\mu_{nf}}{\rho_{nf} c_{pnf}}\left(\frac{\partial u}{\partial y}\right)^2 + \frac{\sigma_{nf} B_0^2 u^2}{\rho_{nf} c_{pnf}}; \tag{3}$$

$$u\frac{\partial C}{\partial x} + v\frac{\partial C}{\partial y} = D_B\frac{\partial^2 C}{\partial y^2} + \frac{D_T}{T_\infty}\frac{1}{\rho_{nf} c_{pnf}}\frac{\partial^2 \hat{h}}{\partial y^2}. \tag{4}$$

The boundary conditions are as follows:

$$u = ax;\ v = 0;\ -\kappa\frac{\partial \hat{h}}{\partial y} = h_f(\hat{h}_f - \hat{h});\ C = C_w(x) \text{ at } y=0; \tag{5}$$

$$u \to 0,\ \hat{h} \to h_\infty,\ C \to C_\infty \text{ as } y \to \infty. \tag{6}$$

In the above equations, u and v denote the velocity components along the x and y directions, respectively. The quantities μ_{nf} and ρ_{nf} represent the dynamic viscosity and density of the nanofluid, respectively, whereas ν_{nf} and ν_f denote the kinematic viscosities of the nanofluid and base fluid, respectively. The parameter β is the Casson fluid parameter, and g denotes the gravitational acceleration. The coefficients β_T and β_C represent the thermal and solutals expansion coefficients, respectively. Furthermore, $\hat{h}_\infty$ denotes the ambient (freestream) volumetric sensible enthalpy, whereas $\hat{h}_w$ represents the wall volumetric sensible enthalpy. The nanoparticle concentration is denoted by C, while C_w and C_∞ corresponds to the wall and freestream concentrations, respectively. In addition, σ_{nf} represents the electrical conductivity of the nanofluid. The parameter B_0 represents the strength of the applied transverse magnetic field, where $(\rho c_p)_{nf}$ represents the effective heat capacity of the nanofluid, and α_{nf} denotes its thermal diffusivity. The thermal conductivity of the base fluid is represented by κ_f. Furthermore, $\hat{h}_f$ represents the volumetric sensible enthalpy evaluated at the fluid-side temperature at the wall, and h_f is the convective heat transfer coefficient. The stretching velocity along the plate is represented by $U_w(x)$ while $C_w(x)$ denotes the nanoparticle concentration distribution along the plate. Finally, the subscripts n_f and b_f correspond to the nanofluid and base fluid, respectively.

In the present investigation, the thermal conductivity of the nanofluid $\kappa(\hat{h})$ was considered to vary linearly with the volumetric sensible enthalpy. Following the modified variable thermal conductivity formulation reported by [36, 37], the effective thermal conductivity is expressed as

$$\kappa(\hat{h}) = \kappa^*(1+\gamma h), \tag{8}$$

where h denotes the dimensionless enthalpy function; κ^* represents the ambient thermal conductivity of the fluid. The thermal conductivity variation parameter is defined as

$$\gamma = \delta \hat{h}_w, \tag{9}$$

where δ is the thermal conductivity variation coefficient m^3/J, which characterizes the sensitivity of the thermal conductivity to changes in the local volumetric sensible enthalpy. Furthermore, the reference thermal diffusivity employed in the non-dimensionalization process is given by

$$\alpha_{nf} = \frac{\kappa^*}{\rho_{nf} c_{p,nf}}. \tag{10}$$

To obtain the transformed nonlinear ordinary differential equations governing the present flow model, the following thermophysical assumptions for the nanofluid were adopted based on the studies of [38–40]; effective density $\rho_{nf} = (1-\varphi)\rho_f + \varphi\rho_p$, dynamic viscosity $\frac{\mu_{nf}}{\mu_{nf} v_{bf}} = \frac{0.904 e^{0.148\varphi}}{1-\varphi+\varphi\frac{\rho_{np}}{\rho_{bf}}}$, (where the present study considers Al_2O_3 nanoparticle volume fractions of $0.01 \le \varphi \le 0.05$). Within this range, increasing nanoparticle loading enhances the effective viscosity of the nanofluid due to stronger nanoparticle–base fluid interactions; specific heat capacity $(\rho c_p) = (1-\varphi)(\rho c_p)_f + \varphi(\rho c_p)_p$, thermal diffusivity $\alpha_{nf} = \frac{\kappa_{nf}}{\rho_{nf} c_{p,nf}}$, and thermal conductivity $\frac{\kappa_{nf}}{\kappa_{bf}} = \frac{\left(\kappa_{np} + 2\kappa_{bf} - 2\varphi(\kappa_{bf} - \kappa_{np})\right)}{\left(\kappa_{np} + 2\kappa_{bf} + \varphi(\kappa_{bf} - \kappa_{np})\right)}$.

The following similarity transformations are introduced to reduce the governing partial differential equations (1)–(4) subject to the boundary conditions (5) and (6)

$$\eta = y\sqrt{\frac{a}{v_f}}; \quad \psi(x,y) = \sqrt{a v_f}\, x f(\eta); \quad u = \frac{\partial \psi}{\partial y}; \quad v = -\frac{\partial \psi}{\partial x}; \tag{11}$$

$$\hat{h} = \hat{h}_w h(\eta); \tag{12}$$

$$C = C_\infty + (C_w - C_\infty)\varphi(\eta). \tag{13}$$

Substituting Equations (8)–(13) into Equations (1)–(4) reveals that Equation (1) is identically satisfied, whereas Equations (2)–(4), together with the boundary conditions (5)–(6), reduce to the following nonlinear ordinary differential equations:

$$\frac{\mu_{nf}}{v_f \rho_{nf}}\left(1+\frac{1}{\beta}\right) f'''(\eta) + f(\eta) f''(\eta) - f'^2(\eta) + Gr_t h + Gr_s \varphi - M f'(\eta) = 0; \tag{14}$$

$$(1+\gamma h) h''(\eta) + \gamma h'^2(\eta) + \mathrm{Pr}_{nf}\, f(\eta) h'(\eta) + Nt\, h'^2(\eta) + Br_h (f''(\eta))^2 + \mathrm{Pr}_{nf}\, M\, Ec_h (f'(\eta))^2 = 0; \tag{15}$$

$$\varphi'' + Scf\, \varphi' + \frac{Nt}{Nb} h'' = 0. \tag{16}$$

Subject to the dimensionless boundary conditions

$$\text{at } \eta=0: \; f(0)=0, \quad f'(0)=1, \quad h'(0) = -Bi(h(0)-\gamma), \quad \varphi(0)=1; \tag{17}$$

$$\text{at } \eta\to\infty: \; f'(\infty)=0, \quad h(\infty)=0, \quad \varphi(\infty)=0; \tag{18}$$

$$Gr_t = \frac{g\beta_T \hat{h}}{\rho_{nf} c_{p,nf} a^2 x}; \quad Gr_s = \frac{g\beta_c (C_w - C_\infty)}{a^2 x}; \quad Br_h = \frac{\mu_{nf} a^2 x^2}{\alpha_{nf} \rho_{nf} c_{p,nf} (\hat{h}_w)} \equiv \frac{\mu_{nf} U^2}{\kappa_{nf} (\hat{h}_w)}; \quad Ec_h = \frac{a^2 x^2}{\rho_{nf} c_{p,nf} \hat{h}_w};$$

$$\mathrm{Pr}_{nf} = \frac{\nu_f}{\alpha_{nf}}; \quad M = \frac{\sigma_{nf} B_0^2}{\rho_{nf}}; \quad \frac{Nt}{Nb} = \frac{D_T \hat{h}_w}{D_B T_\infty \rho_{nf} c_{p,nf} (C_w - C_\infty)}; \quad Sc = \frac{\nu_f}{D_B}; \quad \nu_f = \frac{\mu_f}{\rho_f} \text{ (Ethylene glycol);}$$

$$\frac{\mu_{nf}}{\nu_f \rho_{nf}} = \frac{\mu_{nf}}{(\mu_f / \rho_f)\rho_{nf}} = \frac{\mu_{nf} / \rho_{nf}}{\mu / \rho_f} = \frac{\nu_{nf}}{\nu_f} \neq 1, \text{ such that } \nu_{nf} = \frac{\mu_{nf}}{\rho_{nf}}; \ \nu_f = \frac{\mu_f}{\rho_f}.$$

In order to solve the coupled nonlinear ordinary differential Equations (14)–(16), the equations are transformed into a system of first-order equations, as follows

Such that

$$y_1' = y_2; \tag{20}$$

$$y_2' = y_3; \tag{21}$$

$$y_3' = \frac{-y_1 y_3 + y_2^2 - Gr_t - Gr_s + M y_2}{A}; \tag{22}$$

$$y_4' = y_5; \tag{23}$$

$$y_5' = \frac{-(\gamma + Nt) y_5^2 - \mathrm{Pr}_{nf}\, y_1 y_5 - Br_h y_3^2 - \mathrm{Pr}_{nf}\, MEc_h y_2^2}{1 + \gamma y_4}; \tag{24}$$

$$y_6' = y_7; \tag{25}$$

$$y_7' = -Scy_1 y_7 - \frac{Nt}{Nb} y_5'. \tag{26}$$

The boundary conditions at $\eta \to 0$ are

$$y_1(0) = 0; \quad y_2(0) = 1; \quad y_5(0) = -Bi[y_4(0) - \gamma]; \quad y_6(0) = 1; \tag{27}$$

at $\eta \to \infty$, the conditions are as follows:

$$y_2(\infty) \to 0; \quad y_4(\infty) \to 0; \quad y_6(\infty) \to 0. \tag{28}$$

Where $A = \frac{\nu_{nf}}{\nu_f}\left(1 + \frac{1}{\beta}\right)$. Given the wall flux definitions:

– wall shear stress

$$\tau_w = \mu_{nf} \left(\frac{\partial u}{\partial y}\right)_{y=0}; \tag{29}$$

– wall sensible enthalpy flux

$$q_w'' = -\kappa_w \left(\frac{\partial u}{\partial y}\right)_{y=0} = \frac{-\kappa_w}{\rho_{nf} c_{p,nf}} \left(\frac{\partial \hat{h}}{\partial y}\right)_{y=0}; \tag{30}$$

– wall mass flux

$$j_w'' = -D_{nf} \left(\frac{\partial C}{\partial y}\right)_{y=0} \tag{31}$$

with variable conductivity at the wall, as follows $\kappa_w = \kappa_\infty [1 + \gamma h(0)]$. Differentiating Equations (29)–(31) using the similarity Equations (11)–(13) where, $\hat{h}_\infty = 0$, $\hat{h}_w = \rho_{nf} c_{p,nf} (T_w - T_\infty)$ and evaluate at η=0, the engineering quantities are obtained as

$$C_f \,\mathrm{Re}_x^{1/2} = 2\left(\frac{\mu_{nf}}{\mu_f}\right) f''(0); \tag{32}$$

$$N_u \, \mathrm{Re}_x^{-1/2} = -\left[1 + \gamma h(0)\right] h'(0) ; \tag{33}$$

$$Sh \, \mathrm{Re}_x^{-1/2} = \varphi'(0) . \tag{34}$$

Results and Discussion

This study presents a volumetric sensible enthalpy analysis of magnetohydrodynamic (MHD) Casson nanofluid flow over a stretching sheet, incorporating the effects of thermophoresis and viscous dissipation. The governing partial differential equations (2)–(4), subject to boundary conditions (5)–(6), were transformed using similarity variables (11)–(13) into a coupled system of nonlinear ordinary differential equations (14)–(16) with dimensionless boundary conditions (17)–(18). The coupled equations were further reduced to a system of first-order ODEs and solved numerically using the collocation method implemented in the solve_bvp routine of the SciPy library. The Base physical properties of Al_2O_3-ethylene glycol nanofluid and effects of governing parameters on surface quantities are presented in Tables 3 and 4, whereas the numerical results on the effects of the thermophysical properties on the velocity, enthalpy, and concentration profiles are displayed in Figs. 2–28. The base parameter values, chosen in agreement with the established literature, are β=0.2; Gr_t=5.0; Gr_s=2.0; M=3.0; Ec_h=0.1; Sc=0.62; Br_h=0.01; Nt=0.1; Bi=0.2.

Numerical Validation and Convergence Analysis

The nonlinear ordinary differential equations (14)–(16) were converted into a system of seven first-order differential equations as given in Equations (19)–(26). The resulting boundary-value problem was solved using an adaptive collocation method implemented through SciPy's solve_bvp solver. The solver employs a residual-controlled adaptive mesh refinement technique to achieve accurate solutions while satisfying the boundary conditions given in Equations (27)–(28). To ensure numerical accuracy, the computational domain was selected as $0 \le \eta \le 15$, which was sufficiently large to satisfy the far-field conditions as $f'(\eta) \to 0$, $h(\eta) \to 0$, $\varphi \to 0$. The solver tolerance was set to 10^{-8}, while the maximum number of adaptive mesh nodes was limited to 60,000.

The accuracy of the numerical solutions was monitored through the maximum boundary residual obtained after convergence of the collocation scheme. The solver automatically refined the computational mesh until the prescribed tolerance was achieved (Table 1). For all investigated parameter variations, the maximum boundary residual remained below 3×10^{-13}, indicating excellent satisfaction of the imposed boundary conditions.

The residual values of order 10^{-16} observed for most cases demonstrated that the numerical solutions satisfy the boundary conditions with high precision, while the slightly larger residual observed for the Casson parameter variation (2.85×10^{-13}) remains sufficiently small, confirming the stability of the numerical procedure (Table 2).

Table 1. Boundary condition residuals for parameter variations

Parameter variation	Most frequent residual	Maximum residual
β	1.67×10^{-16}	2.85×10^{-13}
M	1.67×10^{-16}	1.67×10^{-16}
Sc	1.67×10^{-16}	4.46×10^{-14}
Bi	1.67×10^{-16}	3.47×10^{-16}
Gr_t	1.67×10^{-16}	4.52×10^{-15}
Gr_s	1.67×10^{-16}	2.16×10^{-15}
Br_h	1.67×10^{-16}	1.67×10^{-16}
Ec_h	1.67×10^{-16}	9.10×10^{-15}
Nt	1.67×10^{-16}	1.23×10^{-14}

Table 2. Validation of the present numerical method against the classical Newtonian stretching-sheet solution [73]

Quantity	Present result	Exact solution	Error
$f''(0)$	-0.99999956	-1.00000000	4.44×10^{-7}

Table 3. Base physical properties of Al_2O_3-ethylene glycol nanofluid at 25 °C

Property	Ethylene Glycol (Base fluid)	Al_2O_3 (Nanoparticles)
Density ρ, kg/m^3	1110.0	3970.0
Specific heat c_p, (J·K)/kg	2415.0	765.0
Thermal conductivity k, (W·K)/m	0.25	36.00

Table 4. Effects of Governing Parameters on Surface Quantities

Parameter	Value	$h(0)$	$f''(0)$	$Cf\,\mathrm{Re}^{1/2}$	$Nu\,\mathrm{Re}^{1/2}$	$Sh\,\mathrm{Re}^{1/2}$
β	0.1	0.926945	-0.24094	-0.50684	-0.180720	1.064279
	0.2	0.890738	-0.25034	-0.52662	-0.17223	1.026086
	0.5	0.863275	-0.22499	-0.47329	-0.16583	0.992638
	1.0	0.853390	-0.18289	-0.384740	-0.16354	0.979012
M	1	0.318716	-0.19299	-0.40599	-0.04514	0.724094
	2	0.611676	-0.22407	-0.47136	-0.10859	0.879215
	3	0.890738	-0.25034	-0.52662	-0.17223	1.026086
	5	1.421723	-0.29425	-0.61899	-0.30193	1.302501
Sc	0.4	0.937687	-0.17615	-0.37056	-0.18325	0.879377
	0.5	0.912667	-0.21465	-0.45154	-0.17737	0.949346
	0.62	0.890738	-0.25034	-0.52662	-0.17223	1.026086
	0.8	0.867466	-0.29064	-0.61140	-0.16681	1.130142
Bi	0.1	0.900165	-0.24793	-0.52155	-0.08722	0.952957
	0.2	0.890738	-0.25034	-0.52662	-0.17223	1.026086
	0.5	0.863829	-0.25722	-0.54109	-0.41491	1.23560
	1	0.823066	-0.26766	-0.56304	-0.78258	1.555218
Gr_t	1	0.856370	-0.43214	-0.90904	-0.16423	0.9864300
	3	0.873005	-0.34375	-0.72311	-0.16810	1.005678
	5	0.890738	-0.25034	-0.52662	-0.17223	1.026086
	1	0.940545	0.008418	0.017709	-0.18392	1.082883
Gr_s	0.5	0.782656	-0.54867	-1.15419	-0.14722	0.893472
	1	0.820141	-0.44589	-0.93798	-0.15584	0.941525
	2	0.890738	-0.25034	-0.52662	-0.17223	1.026086
	5	1.080566	0.289150	0.608259	-0.21730	1.235119
Nt	0.1	0.890738	-0.25034	-0.52662	-0.17223	1.026086
	0.2	0.956657	-0.108210	-0.22762	-0.18772	1.634849
	0.3	1.023502	0.034576	0.072734	-0.20360	2.340328
	0.4	1.091321	0.178359	0.375198	-0.21990	3.145559
Br_h	0.01	0.890738	-0.25034	-0.52662	-0.17223	1.026086
	0.1	0.891040	-0.250200	-0.52632	-0.17231	1.026264
	0.5	0.892383	-0.249570	-0.52501	-0.17262	1.027054
	1	0.894055	-0.248800	-0.52337	-0.17301	1.028037
Ec_h	0.01	0.082810	-0.556310	-1.17026	0.003466	0.526886
	0.1	0.890738	-0.25034	-0.52662	-0.17223	1.026086
	0.2	2.002887	0.180387	0.379463	-0.456800	1.743620
	0.3	3.414919	0.732324	1.540523	-0.889390	2.690632

Further validation was performed by reducing the present formulation to the classical Newtonian stretching-sheet problem. The limiting case was obtained by removing magnetic effects, buoyancy forces, nanoparticle transport, viscous dissipation, and enthalpy coupling terms, while setting the Casson parameter to the Newtonian limit $\beta\to\infty$. The computed wall shear parameter $f''(0)$ agrees excellently with the exact analytical solution, with an absolute error of 4.44×10^{-7}. This agreement verifies the correctness of the similarity transformation, the implementation of the governing equations, and the reliability of the numerical solver.

The influence of the Casson parameter β on velocity, volumetric sensible enthalpy, and concentration profiles is presented in Figs. 2–4. Increasing β from 0.1 to 1.0 systematically reduced the velocity magnitude throughout the boundary layer as shown in Fig. 2, resulting in a thinner hydrodynamic boundary layer. This occurs because a higher β intensifies the opposing flow interaction, thereby suppressing the fluid momentum near the wall. Fig. 3 shows that increasing β reduces the volumetric sensible enthalpy across the boundary layer, producing a steeper enthalpy gradient and thinner energy-storage boundary layer. This reduction was attributed to the weakened convective transport caused by the suppressed velocity field. In contrast, Fig. 4 reveals a slight enhancement in concentration near the wall with increasing β, as the reduced ve-

locity weakens convective mass transport, allowing diffusion to dominate locally. This leads to modest species accumulation and a slightly thicker concentration-boundary layer. These trends are qualitatively consistent with previously reported Casson fluid and MHD boundary-layer studies [41–44], demonstrating that the volumetric sensible enthalpy formulation captures the same qualitative physics as conventional temperature-based models while providing a direct measure of energy storage per unit volume.

The influence of the magnetic parameter M on the velocity, volumetric sensible enthalpy, and concentration profiles is presented in Figs. 5–7.

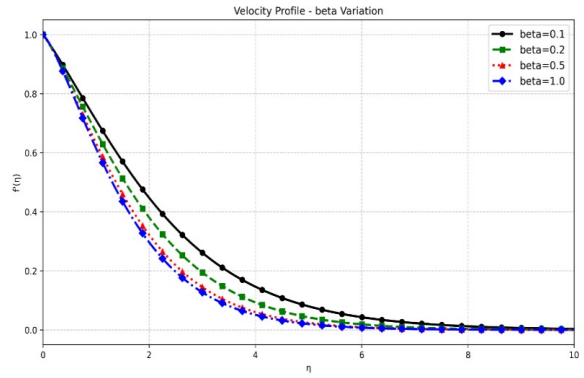


Fig. 2. Effects of β on velocity profiles

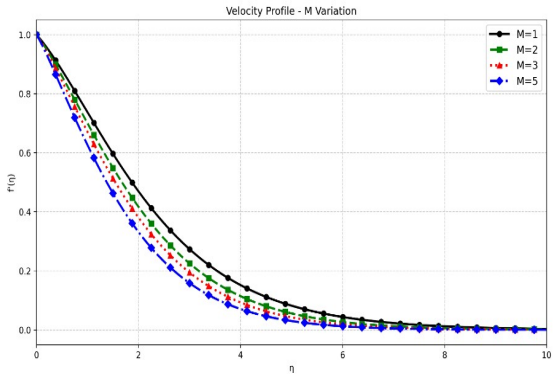


Fig. 5. Effects of M on velocity profiles

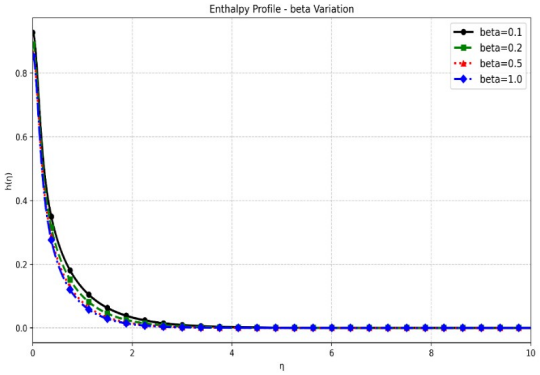


Fig. 3. Effects of β on enthalpy profiles

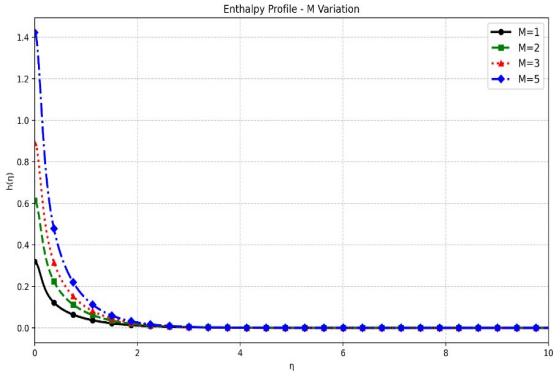


Fig. 6. Effects of M on enthalpy profiles

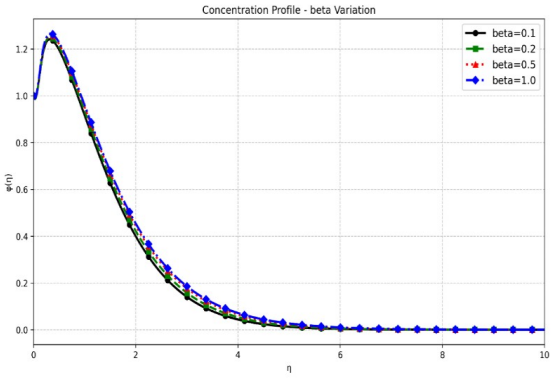


Fig. 4. Effects of β on concentration profiles

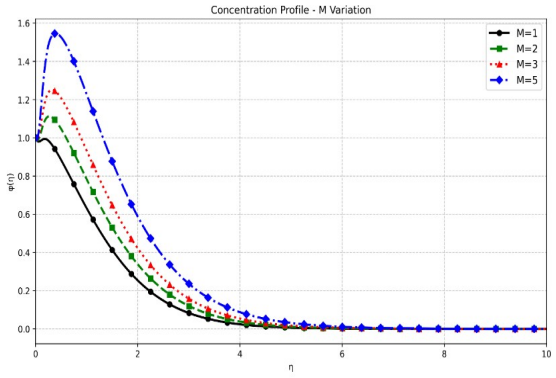


Fig. 7. Effects of M on concentration profiles

Increasing M from 1 to 5 significantly suppressed the velocity throughout the boundary layer, as shown in Fig. 5. The velocity magnitude decreased monotonically, and the decay toward the free-stream condition became more rapid at higher M. This behavior is attributed to the Lorentz force, which acts as a

resistive body force opposing the fluid motion, thereby reducing the momentum transport and thinning the hydrodynamic boundary layer. Fig. 6 revealed an increase in M enhances the volumetric sensible enthalpy distribution within the boundary layer, particularly in the near-wall region. The enthalpy increases owing to Joule heating (Ohmic dissipation), where electrical resistance converts kinetic energy into internal energy. In addition, the suppression of the velocity reduces convective transport, allowing the thermal energy to accumulate near the wall. Consequently, the magnetic field indirectly intensified internal energy generation within the flow domain. An increase in M enhances the concentration distribution across the boundary layer, as shown in Fig. 7. The peak concentration increased, and the decay toward the free-stream condition became more gradual. This is because the Lorentz force reduces the fluid velocity, thereby weakening advective mass transport and allowing molecular diffusion to dominate. Consequently, species accumulation near the wall increased, leading to a thicker concentration boundary layer. These results are consistent with established MHD Casson nanofluid studies [45–48], confirming that the volumetric sensible enthalpy formulation preserves the classical transport behavior observed in conventional temperature-based models while providing a more physically explicit representation of energy storage per unit volume within the boundary layer.

The influence of the Schmidt number Sc on the velocity, volumetric sensible enthalpy, and concentration profiles is shown in Figs. 8–10. Increasing Sc from 0.4 to 0.8 progressively decreased the velocity distribution across the boundary layer, as shown in Fig. 8. A higher Sc corresponds to a reduced mass diffusivity, which weakens the concentration gradients near the wall and diminishes the buoyancy-driven contributions in the momentum equation. Consequently, the hydrodynamic boundary layer became thinner, and the velocity decayed more rapidly away from the wall. In the volumetric Sensible Enthalpy of Fig. 9, an increase in Sc caused a slight but consistent decrease in the enthalpy profile. The reduced mass diffusivity at higher Sc weakened nanoparticle transport and its contribution to energy redistribution, slightly lowering the volumetric sensible enthalpy. The weak sensitivity of $h(\eta)$ compared to the concentration field indicates that heat conduction and viscous dissipation are the dominant energy transport mechanisms. Similarly, the concentration profile of Fig. 10 shows a pronounced decrease as Sc increases. A higher Sc reduces the mass diffusivity, thereby restricting the diffusion of nanoparticle into the free stream. The concentration boundary layer becomes thinner, and the profile decays more rapidly with η. The strong sensitivity of the concentration field to Sc confirms that mass transport is primarily governed by the Schmidt number, and these findings demonstrate that Sc indirectly influences the momentum and enthalpy distributions through coupling effects while directly controlling the concentration boundary layer thickness.

The present observations regarding the Schmidt number effects show qualitative agreement with the trends reported in earlier MHD Casson nanofluid studies [45–50], where increasing Sc, enhances the concentration gradient at the wall. A direct quantitative comparison with these studies is not feasible due to differences in the dimensionless parameter definitions, scaling factors, and the use of an enthalpy-based energy equation in the present work as opposed to the classical temperature-based formulation employed in [45–50]. Therefore, the comparison is presented as a qualitative trend discussion rather than quantitative validation. The accuracy of the numerical method is demonstrated through the convergence analysis presented in Table 1, where the maximum boundary residuals remain below 3×10^{-13} for all parameter variations, confirming the stability and precision of the solve_bvp solver with adaptive mesh refinement and the correctness of the similarity transformation.

The novelty and contribution of the present study lie in the following aspects:

1) Unlike previous studies [45–50], which employed a temperature-based energy equation, the present investigation formulates thermal transport in terms of volumetric sensible enthalpy**,** providing a thermodynamically consistent representation of internal energy storage and redistribution, which is particularly significant for nanofluids where the specific heat varies with nanoparticle concentration.

2) The enthalpy formulation naturally couples' thermophoresis and viscous dissipation effects, offering a more rigorous treatment of thermal transport compared to classical temperature-based models.

3) The present study provides a comprehensive parametric analysis of the enthalpy and concentration distributions (Figs. 2–28), which are not available in [45–50].

4) The combined effects of Casson rheology, MHD, thermophoresis, viscous dissipation, and enthalpy-based energy transport in a unified framework have not been previously reported.

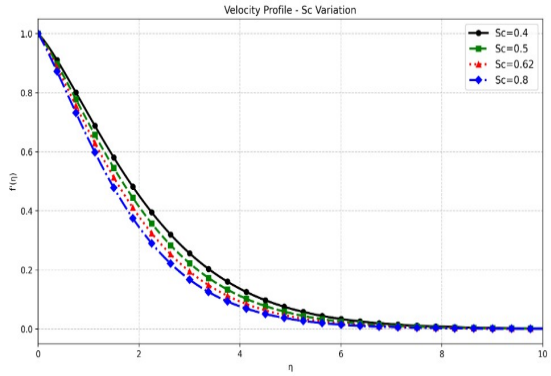


Fig. 8. Effects of Sc on velocity profiles

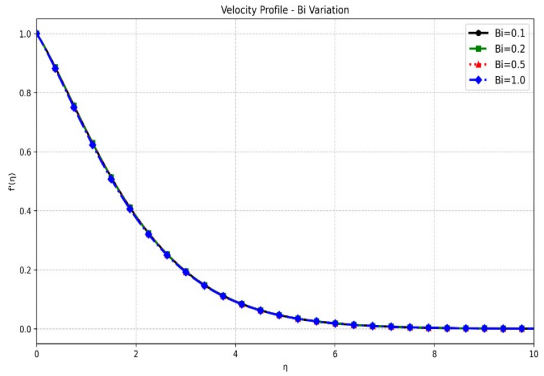


Fig. 11. Effects of Bi on velocity profiles

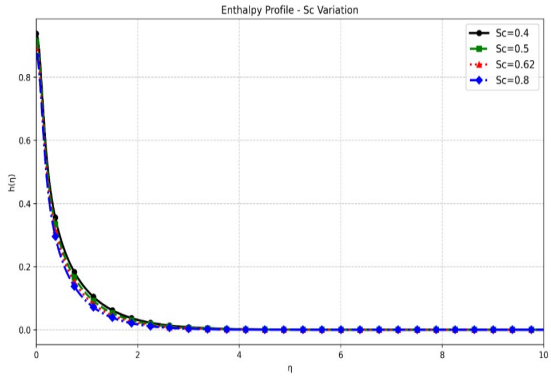


Fig. 9. Effects of Sc on enthalpy profiles

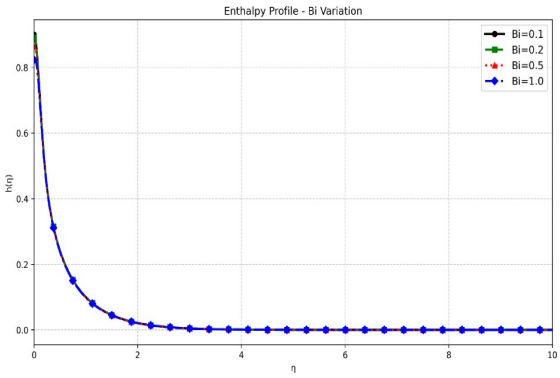


Fig. 12. Effects of Bi on enthalpy profiles

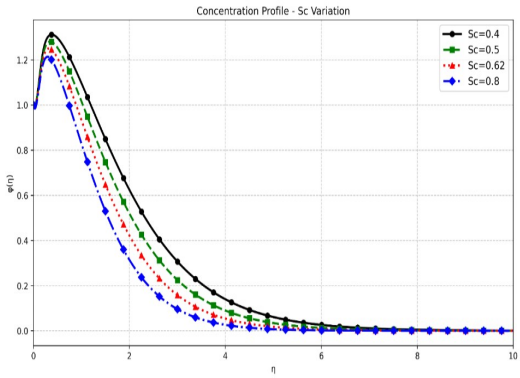


Fig. 10. Effects of Sc on concentration profiles

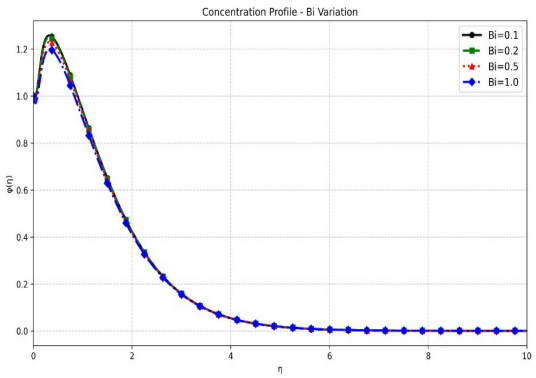


Fig. 13. Effects of Bi on concentration profiles

The influence of the Biot number *Bi* on the velocity, volumetric sensible enthalpy, and concentration profiles is shown in Figs. 11–13. Increasing the Biot number *Bi* from 0.1 to 1.0 produced negligible variations in the velocity profile, as shown in Fig. 11. Because the Biot number appears explicitly in the thermal boundary condition rather than in the momentum equation, its influence on the velocity is only indirect through thermal buoyancy coupling. The nearly overlapping velocity profiles indicate that momentum transport is primarily governed by magnetic, buoyancy, and viscous effects rather than surface convection strength. Fig. 12 shows that increasing slightly *Bi* reduces the near-wall volumetric sensible enthalpy distribution. A larger Biot number corresponds to a stronger convective heat exchange at the surface, which enhances heat removal and reduces the amount of energy stored per unit volume near the wall. The influence of *Bi* remains localized within the thermal boundary layer and diminishes rapidly with increasing η, with all profiles approaching the ambient state at a distance from the surface. The concentration profiles in Fig. 13 exhibit only slight variations, with a small decrease

observed as *Bi* increases. Although the Biot number does not appear directly in the concentration equation, it indirectly affects the concentration through thermal coupling associated with the thermophoresis parameter *Nt*. Enhanced surface heat exchange modifies the enthalpy gradient, inducing a weak thermophoretic response that slightly reduces the nanoparticle concentration near the wall. The proximity of the concentration curves confirms that mass transport is governed predominantly by the Schmidt number effects and solutal buoyancy, whereas surface convection plays a secondary role. The present results are qualitatively comparable to those of earlier investigations on Casson nanofluid [51–54]. Previous temperature-based studies, such as [51], reported enhanced thermal and concentration distributions with increasing *Bi*, whereas the present volumetric sensible enthalpy formulation predicts a slight reduction in the near-wall stored energy owing to enhanced convective heat exchange and reduced local energy retention. Nevertheless, the weak sensitivity of the velocity field and the localization of the Biot number effects within the thermal and concentration boundary layers remain consistent with earlier studies [52–54]. These observations confirm that the Biot number primarily influences thermal and solutal transport near the wall, without significantly altering the bulk momentum field.

The influence of the thermal Grashof number Gr_t on the velocity, volumetric sensible enthalpy, and concentration profiles is shown in Figs. 14–16. Increasing Gr_t from 1 to 10 slightly enhanced the velocity distribution (Fig. 14) owing to buoyancy-driven acceleration, which assisted the flow and strengthened momentum transport within the boundary layer. The enhanced buoyancy force promoted fluid motion, leading to a modest increase in the hydrodynamic boundary layer thickness. Fig. 15 shows a marginal increase in the volumetric sensible enthalpy near the wall as Gr_t increased. Stronger buoyancy-induced convection improves thermal transport from the surface to the fluid, slightly increasing the stored thermal energy per unit volume. However, the relatively weak variation in the enthalpy profiles indicates that heat conduction and viscous dissipation are the dominant thermal transport mechanisms.

In contrast, the concentration profiles in Fig. 16 exhibit a slight decrease with increasing Gr_t. Enhanced buoyancy strengthens convective transport, thereby reducing nanoparticle accumulation near the wall and thinning the concentration boundary layer. This behavior demonstrates that thermal buoyancy indirectly influences species transport through momentum–concentration coupling, primarily affecting the momentum field. The observed enhancement in the velocity with increasing the thermal Grashof number agrees with the results of previous investigations on Casson nanofluids. [55] demonstrated that buoyancy forces significantly enhanced momentum transport in mixed convective MHD Casson nanofluid flow. Similarly, [56] reported that the velocity profile increased with increasing Gr_t. Related studies by [57] and [58] also confirmed that increasing the buoyancy parameters intensifies the fluid motion and thermal boundary layer development. The slight reduction in concentration with increasing Gr_t is also consistent with previously reported behavior in buoyancy-driven nanofluid transport systems, where stronger convection suppresses nanoparticle accumulation near the wall.

The influence of the solutal Grashof number Gr_s on the velocity, volumetric sensible enthalpy, and concentration profiles is shown in Figs. 17–19. Increasing Gr_s from 0.5 to 5.0 significantly enhanced the velocity distribution throughout the boundary layer, as shown in Fig. 17. The solutal Grashof number represents the strength of the buoyancy forces generated by the concentration gradients. Larger values of Gr_s intensify the solutal buoyancy force in the momentum equation, thereby accelerating the fluid motion and strengthening the convective transport within the boundary layer. The influence of solutal buoyancy was most pronounced in the near-wall region, where the concentration gradients were the strongest. Fig. 18 demonstrates a slight increase in the near-wall volumetric sensible enthalpy distribution with increasing Gr_s, accompanied by a marginal thickening of the enthalpy boundary layer. Although Gr_s does not appear explicitly in the energy equation, its influence is transmitted indirectly through an enhanced velocity field. Stronger buoyancy-induced motion increases convective heat transport within the boundary layer, leading to a modest increase in the thermal energy stored per unit volume. Nevertheless, this influence remains secondary compared to the effects of thermal diffusion, viscous dissipation, and other direct thermal transport parameters on Nusselt number.

In contrast, Fig. 19 shows that increasing Gr_s decreases the concentration distribution and thins the concentration boundary layer. Enhanced solutal buoyancy strengthens the convective transport away from the surface, accelerating the nanoparticle migration toward the outer flow region and causing the concentration levels to decay more rapidly with increasing η. The observed enhancement in the velocity with increasing Gr_s number was consistent with previous Casson nanofluid studies. [56] reported that the velocity profile increased with in-

creasing Grashof number. Similarly, [59, 60] confirmed that solutal buoyancy significantly affects the velocity field under mixed convection. Related investigations by [61, 62] also demonstrated that buoyancy forces enhance the momentum transport and indirectly influence the thermal transport characteristics. These findings confirm that the solutal Grashof number primarily governs momentum transport through buoyancy effects, while indirectly influencing the enthalpy and concentration distributions through coupled convective mechanisms.

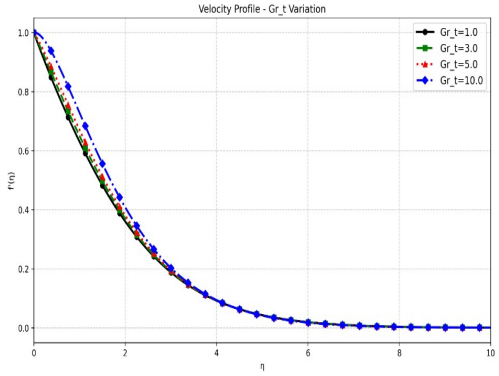


Fig. 14. Effects of Gr_t on velocity profiles

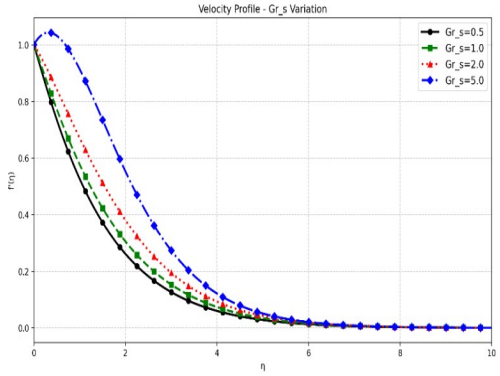


Fig. 17: Effects of Gr_s on velocity profiles

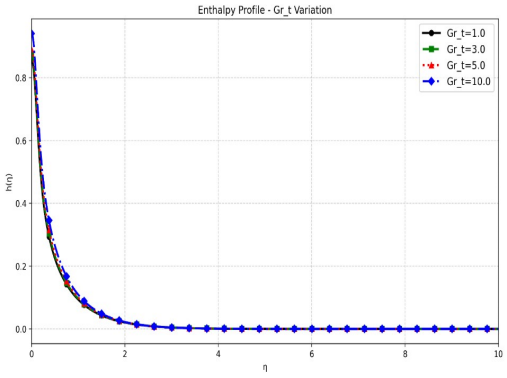


Fig. 15. Effects of Gr_t on enthalpy profiles

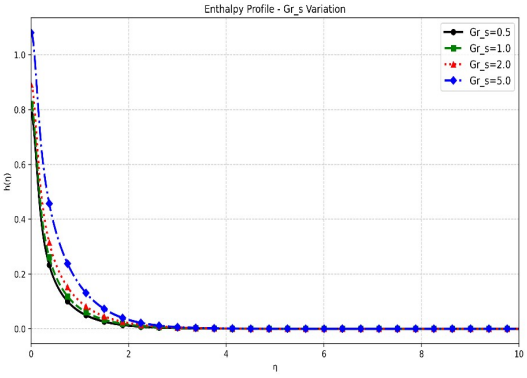


Fig. 18. Effects of Gr_s on enthalpy profiles

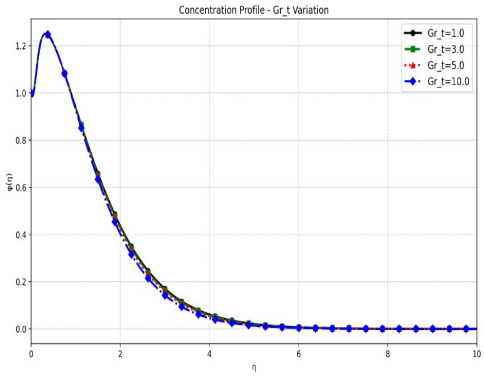


Fig. 16. Effects of Gr_t on concentration profiles

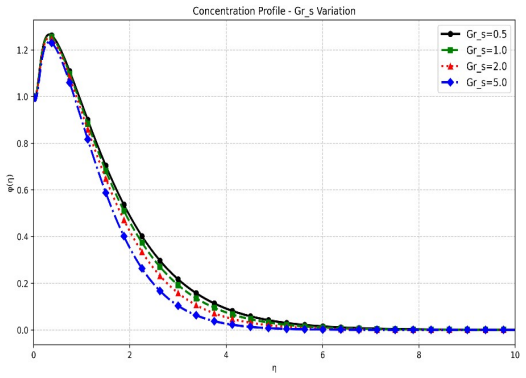


Fig. 19. Effects of Gr_s on velocity profiles

Figs. 20–22 present the influence of the thermophoresis parameter *Nt* on the velocity, volumetric sensible enthalpy, and concentration profiles. Fig. 20 shows that increasing *Nt* slightly enhances the velocity distribution throughout the boundary layer, with the velocity profiles shifting upward as *Nt* increases. Thermophoresis drives nanoparticles from the heated surface toward the cooler regions of the fluid. Although *Nt* does not appear explicitly in the momentum equation, its influence on the velocity field is transmitted indi-

rectly through coupling with the thermal and concentration fields. The migration of nanoparticles modifies the local transport characteristics and reduces the near-wall concentration resistance, thereby slightly enhancing the momentum transport and marginally thickening the hydrodynamic boundary layer.

The volumetric sensible enthalpy profiles presented in Fig. 21 exhibit a noticeable increase with increasing *Nt*. Within the present enthalpy-based framework, $h(\eta)$ represents the thermal energy stored per unit volume. Enhanced thermophoretic transport promotes nanoparticle migration, carrying thermal energy away from the heated surface into the fluid domain, thereby improving thermal energy redistribution and increasing sensible energy storage within the boundary layer. Consequently, the enthalpy boundary layer became slightly thicker as *Nt* increased.

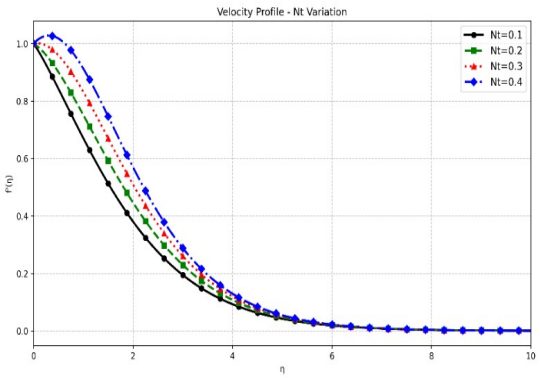


Fig. 20. Effects of Nt on velocity profiles

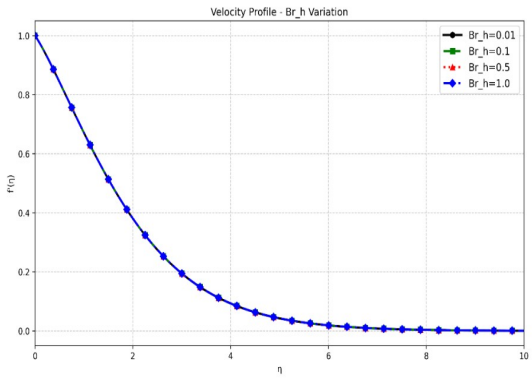


Fig. 23. Effects of Br_h on velocity profiles

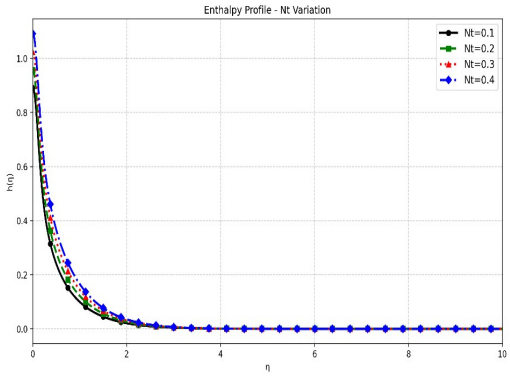


Fig. 21. Effects on enthalpy Nt on enthalpy-based profiles

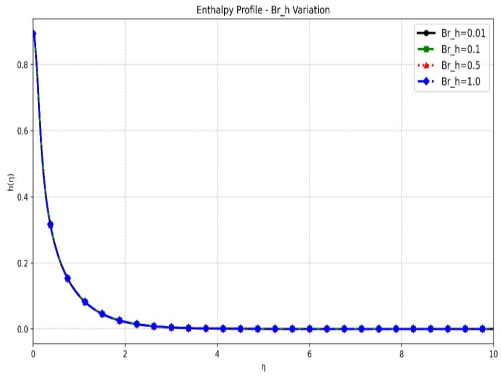


Fig. 24. Effects of Br_h on enthalpy profiles

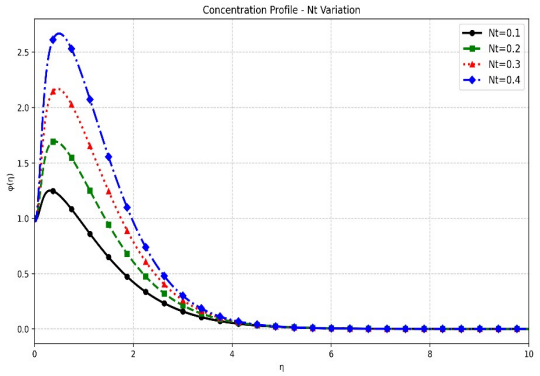


Fig. 22: Effects of Nt on concentration profiles

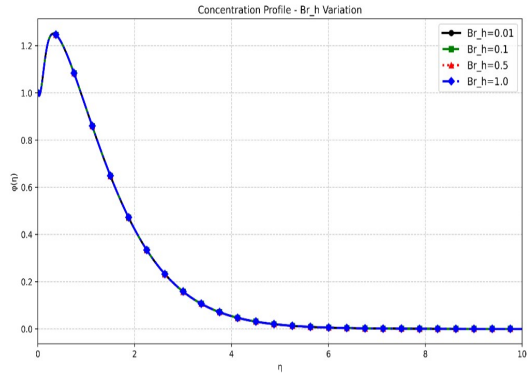


Fig. 25. Effects of Br_h on concentration profiles

Fig. 22 demonstrates that increasing *Nt* significantly enhances the concentration distribution and peak concentration within the boundary layer. Stronger thermophoretic forces intensify nanoparticle migration from the heated wall toward cooler fluid regions, leading to increased particle accumulation within the flow domain and a thicker concentration-boundary layer. At larger similarity distances, all concentration profiles asymptotically approached zero, indicating that the thermophoretic effects diminished far from the surface.

The present results are qualitatively consistent with previous Casson nanofluid studies involving thermophoretic transport effects [63–66], particularly regarding the enhancement of the thermal and concentration distributions with an increase in the thermophoresis parameter. Minor variations in the momentum response may arise owing to the coupled volumetric sensible enthalpy formulation employed in the present analysis. These results confirm that thermophoresis strongly governs nanoparticle transport and indirectly influences momentum and enthalpy distributions through coupled thermal species transport mechanisms within the volumetric sensible-enthalpy framework.

Figs. 23–25 present the influence of the volumetric Brinkman number Br_h on the velocity, volumetric sensible enthalpy, and concentration profiles. In Fig. 23, increasing Br_h from 0.01 to 1.0 produced virtually no noticeable change in the velocity distribution throughout the boundary layer. All the velocity curves completely overlapped from the wall region to the free stream. This behaviour indicates that viscous dissipation, represented by the Brinkman number in the volumetric sensible enthalpy formulation, does not directly influence momentum transport. Because Br_h appears only in the energy equation, the momentum balance governing fluid motion remains essentially unaffected, leading to an invariant velocity boundary layer thickness. In Fig. 24, the enthalpy distributions corresponding to different Br_h values show almost complete overlap across the entire domain, indicating that within the present parameter range, viscous dissipation contributes negligibly to the volumetric sensible enthalpy. The thermal field is predominantly governed by convective and diffusive transport mechanisms, which suppress any observable enhancement owing to viscous heating. Consequently, the enthalpy boundary layer remained unchanged.

In Fig. 25, the concentration curves also completely overlap, demonstrating that changes in viscous dissipation do not significantly affect nanoparticle mass diffusion. Because the concentration equation is only indirectly coupled to the energy field through thermodiffusion mechanisms, the negligible change in enthalpy results in no observable impact on the concentration behaviour. The weak sensitivity of the velocity, volumetric sensible enthalpy, and concentration fields to variations in the Brinkman number Br_h is qualitatively comparable with previous Casson nanofluid studies [67–70], where viscous dissipation effects were found to influence thermal transport primarily under sufficiently large dissipation regimes, whereas momentum and concentration fields remained weakly affected within moderate parameter ranges.

Fig. 26–28 illustrate the influence of the Eckert number Ec_h on the velocity, volumetric sensible enthalpy, and concentration profiles. An increase in Ec_h slightly

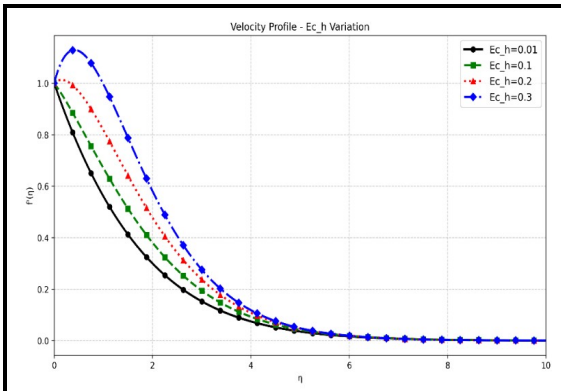


Fig. 26. Effects of Ec_h on velocity profiles

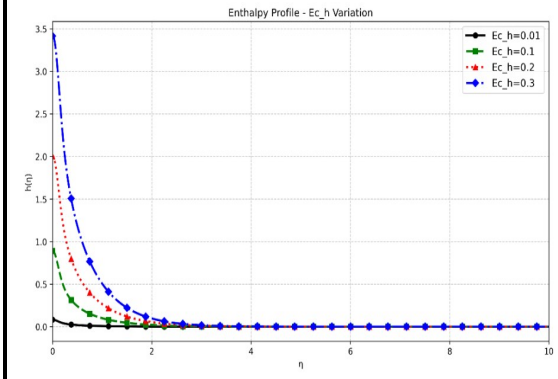


Fig. 27. Effects of Ec_h on enthalpy profiles

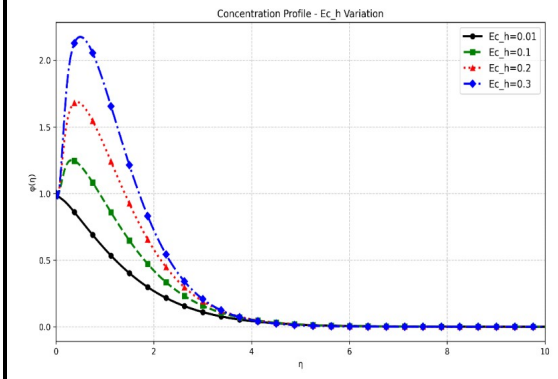


Fig. 28. Effects of Ec_h on concentration profiles

enhanced the velocity distribution (Fig. 26) owing to the indirect thermal–momentum coupling generated by viscous dissipation. Although Ec_h does not appear explicitly in the momentum equation, the increase in volumetric sensible enthalpy strengthens the buoyancy effects, resulting in mild flow acceleration and slight thickening of the momentum boundary layer. Fig. 27 shows that the volumetric sensible enthalpy increases significantly with increasing Ec_h, indicating enhanced thermal energy storage per unit volume as viscous dissipation acts as an internal volumetric heat source within the boundary layer. In Fig. 28, increasing Ec_h enhances the nanoparticle concentration and slightly thickens the concentration boundary layer owing to the intensified thermophoretic transport induced by stronger enthalpy gradients. Overall, viscous dissipation enhances thermal energy transport and indirectly strengthens the momentum and concentration distributions through coupled buoyancy and thermophoretic mechanisms within the volumetric sensible enthalpy framework. The influence of viscous dissipation (Eckert number) on enhancing thermal energy and modifying boundary layer characteristics has been widely reported in previous studies on MHD nanofluid flows [70–72], where it was shown that viscous heating significantly increases the thermal energy distribution while exerting only indirect effects on momentum and mass transport through thermal–species coupling mechanisms.

Summary and Conclusion

This study investigated the effects of several governing parameters on the velocity, volumetric sensible enthalpy, and concentration distributions in MHD Casson nanofluid flow using a volumetric sensible enthalpy formulation. The results revealed the following:

1. Increasing the Casson parameter β decreases the velocity, and volumetric sensible enthalpy while slightly increasing the concentration owing to reduced convective transport.

2. Increasing the magnetic parameter M suppresses the velocity but enhances the volumetric sensible enthalpy and concentration because of the Lorentz force effects and Joule heating.

3. Increasing the Schmidt number Sc decreases the velocity, volumetric sensible enthalpy, and concentration, with the strongest reduction occurring in the concentration boundary layer owing to lowering the mass diffusivity.

4. Increasing the Biot number Bi produces negligible changes in velocity but slightly decreases the volumetric sensible enthalpy and concentration near the wall through enhanced surface heat exchange.

5. Increasing the thermal Grashof number Gr_t enhances the velocity and slightly increases the volumetric sensible enthalpy while reducing the concentration owing to buoyancy-driven convection.

6. Increasing the solutal Grashof number Gr_s significantly enhances the velocity, slightly increases the volumetric sensible enthalpy, and decreases the concentration through stronger solutal buoyancy effects.

7. Increasing the thermophoresis parameter Nt enhances the velocity, volumetric sensible enthalpy, and concentration by intensifying nanoparticle migration and thermal energy transport.

8. Increasing the volumetric Brinkman number Br_h has a negligible effect on the velocity, volumetric sensible enthalpy, and concentration within the investigated parameter range.

9. Increasing the Eckert number Ec_h enhances volumetric sensible enthalpy and slightly increases both velocity and concentration owing to viscous dissipation effects.

They have important applications in several engineering and industrial processes, including thermal energy storage and heat exchanger systems, cooling technologies involving nanofluids in electronic and microelectronic devices, polymer extrusion, coating, and stretching sheet manufacturing processes, metallurgical and materials processing industries involving electrically conducting fluids, biomedical engineering applications involving Casson fluid behavior such as blood flow analysis, solar thermal collectors, and renewable energy systems. Nuclear reactor cooling and high-temperature energy transportation systems. MHD pumps, generators, flow control devices, chemical processing and nanoparticle transport technologies, aerospace and automotive thermal management systems, and industrial processes involving viscous dissipation, thermophoresis, and mixed convection transport phenomena.

Nomenclature

h – dimensionless enthalpy $h = \dfrac{\hat{h} - \hat{h}_\infty}{\hat{h}_w - \hat{h}_\infty} = \dfrac{\hat{h}}{\hat{h}_w} = \dfrac{T - T_\infty}{T_w - T_\infty} = \theta$;

$\hat{h}$ – dimensional volumetric sensible enthalpy $\hat{h} = \rho_{nf} c_{p,nf} (T - T_\infty)$;

$\hat{h}_w$ – wall stream volumetric sensible enthalpy $\hat{h}_w = \rho_{nf} c_{p,nf} (T_w - T_\infty)$;

$\hat{h}_\infty$ – free stream volumetric sensible enthalpy $\hat{h}_\infty$=0;

T – local temperature field $T = T_\infty + \dfrac{\hat{h}}{\rho_{nf} c_{p,nf}}$.

Data Availability Declarations

The present work is theoretical in nature. All data and parameters employed were derived from existing peer-reviewed publications and modified for modeling purposes. No experimental data were produced. The modified data is available. References to the original data sources are provided within the manuscript.

Acknowledgements

The authors thank the reviewers and the editorial team for their constructive comments on improving the quality of this article.

Funding Statement

This research did not receive any specific grant from funding agencies in the public, commercial, or not-for-profit sectors.

Conflict of Interest

This study received no external funding.

Authors Contribution Statement

Tega Felix Onojovwo, is the first author, did the conceptualization, analysis, and writing of the original draft.

Anselm Onyekachukwu Oyem is the corresponding author, contributed to the conceptualization, supervision of the manuscript, project administration, validation, review and editing.

Imoni Sunday Obomeviekome supervised and edited.

Gyegwe Jessica Mrumun edited and supervised.

Clinical Trial

We hereby state that the study is **not a clinical trial**, hence, it is NOT APPLICABLE.

Consent to Publish Declaration

The authors consent to the publication of the manuscript

Ethics and Consent to Participate Declarations

This study did not involve human participants or animals; therefore, ethical approval was not required.

References

1. Okonkwo, E. C., Wole-Osho, I., & Al-Ansari, T. (2021). An updated review of nanofluids in various heat transfer devices. *Journal of Thermal Analysis and Calorimetry*, vol. 145, iss. 6, pp. 2817–2872. https://doi.org/10.1007/s10973-020-09760-2.
2. Kleinstreuer, C. & Feng, Y. (2011). Experimental and theoretical studies of nanofluid thermal conductivity enhancement: A review. *Nanoscale Research Letters*, vol. 6, article 229. https://doi.org/10.1186/1556-276X-6-229.
3. Sridhara, V. & Satapathy, L. N. (2011). Al_2O_3-based nanofluids: A review. *Nanoscale Research Letters*, vol. 6, article 456. https://doi.org/10.1186/1556-276X-6-456.
4. Hemmat Esfe, M., Karimipour, A., Yan, W.-M., Akbari, M., Safaei, M. R., & Dahari, M. (2015). Experimental study on thermal conductivity of ethylene glycol based nanofluids containing Al_2O_3 nanoparticles. *International Journal of Heat and Mass Transfer*, vol. 88, pp. 728–734. https://doi.org/10.1016/j.ijheatmasstransfer.2015.05.010.
5. Xu, J., Bandyopadhyay, K., & Jung, D. (2016). Experimental investigation on the correlation between nanofluid characteristics and thermal properties of Al_2O_3 nanoparticles dispersed in ethylene glycol–water mixture. *International Journal of Heat and Mass Transfer*, vol. 94, pp. 262–268. https://doi.org/10.1016/j.ijheatmasstransfer.2015.11.056.

6. Sundar, L. S., Ramana, E. V., Singh, M. K., & Sousa, A. C. M. (2014). Thermal conductivity and viscosity of stabilized ethylene glycol and water mixture Al_2O_3 nanofluids for heat transfer applications: An experimental study. *International Communications in Heat and Mass Transfer*, vol. 56, pp. 86–95. https://doi.org/10.1016/j.icheatmasstransfer.2014.06.009.
7. Zakaria, I., Azmi, W. H., Mohamed, W. A. N. W., Mamat, R., & Najafi, G. (2015). Experimental investigation of thermal conductivity and electrical conductivity of Al_2O_3 nanofluid in water–ethylene glycol mixture for proton exchange membrane fuel cell application. *International Communications in Heat and Mass Transfer*, vol. 61, pp. 61–68. https://doi.org/10.1016/j.icheatmasstransfer.2014.12.015.
8. Adogbeji, V. O., Atofarati, E. O., Sharifpur, M., & Meyer, J. P. (2025). Magnetohydrodynamics of nanofluid internal forced convection: A review and outlook for practical applications. *Results in Physics*, vol. 68, article 108082. https://doi.org/10.1016/j.rinp.2024.108082.
9. Abd Elfatah, M. G., Abd-Ellatif, O. E., Attia, A. A. A., & Elnady, A. O. (2024). State of art on the role of using a nanofluid in enhancing heat transfer in microchannels with different geometries. *Journal of Engineering and Applied Science*, vol. 71, article 218. https://doi.org/10.1186/s44147-024-00557-w.
10. Sowmiya, C., Rushi Kumar, B., Bég, O. A., & Kuharat, S. (2024). Modeling and analysis of MHD free convective thermo-solutal transport in Casson fluid flow with radiative heat flux. *Journal of Thermal Analysis and Calorimetry*, vol. 149, pp. 6195–6209. https://doi.org/10.1007/s10973-024-13115-6.
11. Casson, N. (1959). A flow equation for pigment-oil suspensions of the printing ink type. In: Mill, C. C. (ed.) Rheology of Disperse Systems. London: Pergamon Press, pp. 84–104.
12. Khan, D. & Ali, G. (2024). Comparative study of dusty tetra hybrid Casson nanofluid flowing in a generalized two-phase MHD medium between parallel microplates with a porous medium. *European Physical Journal Special Topics*, vol. 233, pp. 2225–2243. https://doi.org/10.1140/epjs/s11734-024-01184-5.
13. Reddy, M. V., Vajravelu, K., Lakshminarayana, P., & Sucharitha, G. (2024). Heat source and Joule heating effects on convective MHD stagnation point flow of Casson nanofluid through a porous medium with chemical reaction. *Numerical Heat Transfer, Part B: Fundamentals*, vol. 85, iss. 3, pp. 286–304. https://doi.org/10.1080/10407790.2023.2233694.
14. Khan, W., Khan, W., Hussain, S., & Salah, B. (2024). A mathematical model of Casson nanofluid flow over a vertically stretched porous surface along with bioconvection, Joule heating and thermal Robin conditions. *Journal of Applied Mathematics and Mechanics*, vol. 165, iss. 9. https://doi.org/10.1177/16878132241275435.
15. Olkha, A. & Choudhary, R. (2024). Numerical simulation of MHD radiative Casson nanofluid flow over a nonlinearly heated stretching sheet embedded in porous medium. *Journal of Computational and Theoretical Transport*, vol. 53, iss. 3, pp. 184–206. https://doi.org/10.1080/23324309.2024.2332677.
16. Huang, J. S. & Wang, X. W. (2026). Analysis of heat and mass transfer in nanofluid flow over a stretching surface in a porous medium considering thermophoretic and Darcy effects. *Boundary Value Problems*, vol. 2026, article 111. https://doi.org/10.1186/s13661-026-02299-5.
17. Talukdar, B. & Pal, D. (2025). Induced magnetic field effects on thermophoretic and visco-dissipative chemically reactive thermo-radiative flows. *Thermal Advances*, vol. 4, article 100054. https://doi.org/10.1016/j.thradv.2025.100054.
18. Alao, S., Abdulkareem, F. A., Ogunmola, O. J., & Oderinu, R. A. (2026). Theoretical investigation of heat and mass transfer in unsteady magnetohydrodynamic Williamson nanofluid flow past a permeable stretching surface with viscous dissipation effect. *Thermal Advances*, vol. 6, article 100101. https://doi.org/10.1016/j.thradv.2026.100101.
19. Alrihieli, H. & Aldhabani, M. S. (2025). Analysis of dissipative slip flow in couple stress nanofluids over a permeable stretching surface for heat and mass transfer optimization. *Case Studies in Thermal Engineering*, vol. 67, article 105819. https://doi.org/10.1016/j.csite.2025.105819.
20. Yasmin, H. (2025). Enhanced thermal analysis of bioconvective magnetized Ree–Eyring nanofluid flow on a stretching sheet with Cattaneo–Christov heat flux and microorganism dynamics. *Case Studies in Thermal Engineering*, vol. 68, article 106814. https://doi.org/10.1016/j.csite.2025.106814.
21. Panda, S., Shamshuddin, M. D., Obalalu, A. M., Salawu, S. O., & Mishra, S. R. (2025). Cattaneo–Christov hypothesis in a micropolar nanofluid flow over a stretching sheet subjected to exponential space-based heat generation and bilateral reactions. *Case Studies in Thermal Engineering*, vol. 68, article 106813. https://doi.org/10.1016/j.csite.2025.106813.
22. Reddy, G. J., Deepthi, V. V. L., Raju, R. S., Reddy, B. M., & Ali, F. (2025). Computational modelling of thermal and mass transport in MHD nanofluid flow across a non-linear surface with chemical response and viscous dissipation. *Modeling Earth Systems and Environment*, vol. 11, article 254. https://doi.org/10.1007/s40808-025-02440-w.
23. Hussain, Z., Ayaz, M., Islam, S., Abualnaja, K. M., & Sulaiman, M. (2025). Heat and mass transfer analysis of MHD hybrid nanofluid flow with microorganism over a bi-directional stretching sheet: Effects of thermophoresis and Brownian motion. *International Journal of Dynamics and Control*, vol. 8, article 306. https://doi.org/10.1007/s41939-025-00880-6.

24. Verma, D. & Mehta, R. (2026). Numerical investigation of micropolar aluminum oxide nanofluid flow over an inclined stretching sheet. *Discover Applied Sciences*, vol. 8, article 311. https://doi.org/10.1007/s42452-026-08268-y.
25. Reddy, G. J., Mangathai, P., & Pothanna, N. (2024). Analysis of heat generation impact on nanofluid flow over a stretching sheet. *Partial Differential Equations in Applied Mathematics*, vol. 11, article 10085. https://doi.org/10.1016/j.padiff.2024.100852.
26. Priyadharshini, P., Karpagam, V., Shah, N. A., & Alshehri, M. H. (2023). Bio-convection effects of MHD Williamson fluid flow over a symmetrically stretching sheet: machine learning. *Symmetry*, vol. 15, iss. 9, article 1684. https://doi.org/10.3390/sym15091684.
27. Sankari, M. S., Rao, M. E., Awwad, F. A., Ismail, E. A. A., Makinde, O. D., & Khan, W. (2025). Influence of dual stratification on the magnetohydrodynamic flow of Jeffrey nanofluid over an exponentially stretching permeable sheet with viscous dissipation and Joule heating. *Frontiers in Chemistry*, vol. 12, article 1451053. https://doi.org/10.3389/fchem.2024.1451053.
28. Kamath, A. V., Puneeth, V., & Nisar, K. S. (2025). Modeling and analysis of the bioconvective flow of nanofluid over a stretching sheet with Thompson–Troian slip condition. *Journal of Thermal Analysis and Calorimetry*, vol. 150, iss. 26, pp. 14921–14931. https://doi.org/10.1007/s10973-025-14921-2.
29. Preeti, Sharma, P., Chaudhary, R., Sharma, B. K., Govind, & Meena, R. R. (2026). Investigation of Brownian motion/thermophoresis impacts on radiative viscoelastic chemically reactive magnetite fluid flow on a stretching sheet. *Discover Applied Sciences*, vol. 8, article 608. https://doi.org/10.1007/s42452-026-08596-z.
30. Khader, M. M., Adel, M., Babatin, M. M., & Alaidrous, A. (2025). Williamson nanofluid flow and thermal transfer generated by a convectively heated stretched sheet via Fibonacci–Luca's polynomials. *AIMS Mathematics*, vol. 10, iss. 12, pp. 29012–29036. https://doi.org/10.3934/math.20251276.
31. Khalila, K. M., Mohammed, F. A., Abbas, W., & Megahed, A. M. (2025). Exploring slip boundary impacts on magnetohydrodynamic Casson nanofluid flow over a vertical stretching sheet with nonlinear thermal radiation. *Journal of Taibah University for Science*, vol. 19, iss. 1. https://doi.org/10.1080/16583655.2025.2565855.
32. Sankari, M. S., Rao, M. E., Shams, Z. E., Algarni, S., Sharif, M. N., Alqahtani, T., Eid, M. R., Jamshed, W., & Irshad, K. (2024). Williamson MHD nanofluid flow via a porous exponentially stretching sheet with bioconvective fluxes. *Case Studies in Thermal Engineering*, vol. 59, article 104453. https://doi.org/10.1016/j.csite.2024.104453.
33. Liu, Q., He, Y.-L., & Li, Q. (2017). Enthalpy-based multiple-relaxation-time lattice Boltzmann method for solid-liquid phase-change heat transfer in metal foams. *Physical Review E*, vol. 96, iss. 2, article 023303. https://doi.org/10.1103/PhysRevE.96.023303.
34. Ramakrishnan, T. & Bhalla, A. P. S. (2023). A low Mach enthalpy method to model non-isothermal gas–liquid–solid flows with melting and solidification. *International Journal of Multiphase Flow*, vol. 169, article 104605. https://doi.org/10.1016/j.ijmultiphaseflow.2023.104605.
35. Santos, A. C., Sacomano Filho, F. L., & Vié, A. (2023). The general formulation of the energy equation and the impact of enthalpy diffusion on multi-component droplet heat and mass transfer. *International Journal of Heat and Mass Transfer*, vol. 210, article 124172. https://doi.org/10.1016/j.ijheatmasstransfer.2023.124172.
36. Elbashbeshy, E. M. A. & Ibrahim, F. N. (1993). Steady free convection flow with variable viscosity and thermal diffusivity along a vertical plate. *Journal of Physics D: Applied Physics*, vol. 26, iss. 12, article 2137. https://doi.org/10.1088/0022-3727/26/12/007.
37. Seddeek, M. A. & Abdelmeguid, M. S. (2006). The effects of radiation and thermal diffusivity on heat transfer over stretching surface with variable heat flux. *Physics Letters A*, vol. 348, iss. 3–6, pp. 172–179. https://doi.org/10.1016/j.physleta.2005.01.101.
38. Xuan, Y. & Roetzel, W. (2000). Conceptions for heat transfer correlation of nanofluids. *International Journal of Heat and Mass Transfer*, vol. 43, iss. 19, pp. 3701–3707. https://doi.org/10.1016/S0017-9310(99)00369-5.
39. Pak, P. C. & Cho, Y. I. (1998). Magnetohydrodynamic and heat transfer of dispersed fluids with submicron metallic oxide particles and experimental heat transfer. *Journal of Thermal Energy Generation, Transport, Storage, and Conversion*, vol. 11, iss. 2, pp. 151–170. https://doi.org/10.1080/08916159808946559.
40. Maiga, S. E. B., Nguyen, C. T., Galanis, N., & Roy, G. (2004). Heat transfer behaviours of nanofluids in a uniformly heated tube. *Superlattices and Microstructures*, vol. 35, iss. 3–6, pp. 543–557. https://doi.org/10.1016/j.spmi.2003.09.012.
41. Asogwa, K. K. & Ibe, A. A. (2020). A study of MHD Casson fluid flow over a permeable stretching sheet with heat and mass transfer. *Journal of Engineering Research and Reports*, vol. 16, iss. 2, pp. 10–25. https://doi.org/10.9734/JERR/2020/v16i217161.
42. Kasali, K. B., Gbadamosi, B., Familua, A. B., & Tairu, M. L. (2024). Heat and mass transfer of an MHD Casson fluid with variable properties and non-linear thermal radiation over an elastic sheet. *Journal of Applied and Physical Sciences*, vol. 2, no. 1, pp. 80–87.

43. Das, U. J. (2021). MHD boundary layer flow of Casson fluid past an inclined plate in the presence of Soret / Dufour effects, heat source and first-order chemical reaction. *Journal of Scientific Research*, vol. 13, no. 3, pp. 785–795. https://doi.org/10.3329/jsr.v13i3.52234.
44. Puneeth, V., Manjunatha, S., Madhukesh, J. K., & Ramesh, G. K. (2021). Three-dimensional mixed convection flow of hybrid Casson nanofluid past a non-linear stretching surface: a modified Buongiorno's model aspects. *Chaos, Solitons and Fractals*, vol. 152, article 111428. https://doi.org/10.1016/j.chaos.2021.111428.
45. Abbas, N., Shatanawi, W., Hasan, F., & Shatnawi, T. A. M. (2024). Investigation of MHD radiative Casson micropolar hybrid nanofluid over exponential curved stretching sheet. *Journal of Radiation Research and Applied Sciences*, vol. 18, iss. 1, article 101269. https://doi.org/10.1016/j.jrras.2024.101269.
46. Kumar, V. V. & Raja Shekar, M. N. (2024). Heat and mass transfer in radiative MHD Casson nanofluid flow over a nonlinear stretching sheet. *International Journal of Applied Mathematics*, vol. 37, no. 6S, article 1893. https://doi.org/10.12732/ijam.v37i6s.1893.
47. Manthramurthy, P. & Vempati, S. R. (2025). Significance of multiple slips and thermal radiation on heat and mass transfer in MHD Casson nanofluid flow over an exponentially stretching porous sheet with non-uniform heat source and sink. *Multiscale and Multidisciplinary Modeling, Experiments and Design*, vol. 8, article 157. https://doi.org/10.1007/s41939-025-00743-0.
48. Vinutha, K., Madhukesh, J. K., Prasad, K. V., Kulshreshta, A., Shah, N. A., & Yar, M. (2025). MHD Casson nanofluid flow over a three-dimensional exponentially stretching surface with waste discharge concentration: A revised Buongiorno's model. *Applied Rheology*, vol. 35, no. 1, pp. 20250040. https://doi.org/10.1515/arh-2025-0040.
49. Algehyne, E. A., Yasmin, H., Alduais, F. S., Al-Bossly, A., & Khan, A. (2026). Thermal analysis of Cattaneo–Christov heat/mass flux model effects on radiative Casson nanofluid flow past a bi-directional extending sheet subject to exponential heat source with machine learning approach. *Open Physics*, vol. 24, no. 1, pp. 20250254. https://doi.org/10.1515/phys-2025-0254.
50. Prakash, O. (2025). Dissipative stagnation point flow of the Casson nanofluid over a stretching sheet under the influence of porous media, binary chemical reaction and variable surface heat flux condition. *Pramana – Journal of Physics*, vol. 99, article 31. https://doi.org/10.1007/s12043-024-02873-5.
51. Aroloye, S. J., Fenuga, O. J., & Abiala, I. O. (2025). Analysis of radiative hydromagnetic Casson nanofluid flow with convective boundary condition. *Ife Journal of Science*, vol. 27, no. 1. https://doi.org/10.4314/ijs.v27i1.2s.
52. Khan, A., Hashim, Farooq, M., Hussain, S.M., Ahmad, H., Jamshed, W., Eid, M. R., & Abdalla, N. S. E. (2025). Heat and mass transfer in magnetic Casson nanofluids flow with radiation and stratification effects: Thermal management applications. *Journal of Radiation Research and Applied Sciences*, vol. 18, iss. 4, article 102019. https://doi.org/10.1016/j.jrras.2025.102019.
53. Vinodkumar Reddy, M., Lakshminarayana, P., Vajravelu, K., & Sucharitha, G. (2025). Activation of energy in MHD Casson nanofluid flow through a porous medium in the presence of convective boundary conditions and suction/injection. *Numerical Heat Transfer Part A: Applications*, vol. 86, iss. 5, pp. 1069–1085. https://doi.org/10.1080/10407782.2023.2271655.
54. Priyadharshini, P., Sowndharya, M., & Chamkha, A. J. (2025). Thermal and flow analysis of chemically reactive Casson hybrid nanofluids with machine learning validation. *Mechanics of Time-Dependent Materials*, vol. 29, article 74. https://doi.org/10.1007/s11043-025-09812-w.
55. Duguma, K. A. (2026). Effects of buoyancy on radiative MHD mixed convective flow of Casson nanofluid across a preamble slippery sheet in Darcy-Forchheimer porous medium: Shrinking/stretching surface mode. *Numerical Heat Transfer, Part B: Fundamentals*, vol. 87, iss. 1. https://doi.org/10.1080/10407790.2025.2532116.
56. Saleem, M., Al-Zubaidi, A., Tufail, M. N., Fiaz, Z., & Saleem, S. (2024). Exploration of numerical simulation for unsteady Casson nanofluid thin film flow over stretching surface with mixed convection effects using Buongiorno's nanofluid model. *ZAMM – Zeitschrift für Angewandte Mathematik und Mechanik*, vol. 104, iss. 12, article e202400165. https://doi.org/10.1002/zamm.202400165.
57. Javid, K., Akbar, N. S., Shaiq, S., Khan, A., Jamshed, W., Hussain, S. M., Guedri, K., Ahmad, H., & Abd-Elmonem, A. (2026). MHD Casson nanofluid flow over a vertical stretchable sheet saturated with a porous medium: A parametric approach for sensitive analysis. *Discover Nano*, vol. 21, article 209. https://doi.org/10.1186/s11671-026-04667-7.
58. Seada, M. M. & Saeed, A. (2026). Thermal analysis of Casson hybrid nanofluid flow with solar radiation and inclined magnetic field. *Chemical Engineering and Technology*, vol. 49, iss. 3, article e70203. https://doi.org/10.1002/ceat.70203.
59. Samaila, G. & Jha, B. K. (2025). Heat and mass transfer mixed convection Casson MHD nanofluid flow over a vertical plate with nonlinear thermal radiation. *SSRN*, 32 p. https://doi.org/10.2139/ssrn.5391612.

60. Ajithkumar, M. (2025). Thermo-solutal dynamics of electroactive Casson nanofluid flow through an uneven asymmetric conduit for advanced microfluidic applications. *Advanced Theory and Simulations*, vol. 8, no. 12, article e01148. https://doi.org/10.1002/adts.202501148.
61. Akolade, M. T. & Idowu, A. S. (2025). Radiation effect on gravity-driven nanofluid flow over a convective heated wall: RSM and ANN prediction analysis. *Nano-Structures and Nano-Objects*, vol. 43, article 101506. https://doi.org/10.1016/j.nanoso.2025.101506.
62. Enyadene, L. G., Rikitu, E. H., & Gabissa, A. F. (2023). Numerical investigation of heat and mass transfer of variable viscosity Casson nanofluid flow through a microchannel filled with a porous medium. *Journal of Applied Math*, vol. 1, no. 3, article 194. https://doi.org/10.59400/jam.v1i3.194.
63. Kumar, J., Chand, K., & Thakur, P. (2026). Numerical study of hall current and thermophoresis effect on the hydromagnetic Casson nanofluid flow over a stretching surface. *Journal of the Nigerian Society of Physical Sciences*, vol. 8, iss. 2, article 3259. https://doi.org/10.46481/jnsps.2026.3259.
64. Khan, S., Kumar, D., Kumar, R., & Mehta, R. (2025). Study of unsteady Casson nanofluid flow across a stretching surface embedded in a porous medium in the presence of Stefan blowing and radiation. *Journal of Thermal Analysis and Calorimetry*, vol. 150, pp. 22363–22373. https://doi.org/10.1007/s10973-025-14778-5.
65. Tawade, J. V., Guled, C. N., Noeiaghdam, S., Fernandez-Gamiz, U., Govindan, V., & Balamuralitharan, S. (2022). Effects of thermophoresis and Brownian motion for thermal and chemically reacting Casson nanofluid flow over a linearly stretching sheet. *Results in Engineering*, vol. 15, article 100448. https://doi.org/10.1016/j.rineng.2022.100448.
66. Paul, A., Sarma, N., & Patgiri, B. (2025). Thermal and mass transfer analysis of Casson-Maxwell hybrid nanofluids through an unsteady horizontal cylinder with variable thermal conductivity and Arrhenius activation energy. *Numerical Heat Transfer Part A: Applications*, vol. 86, iss. 9, pp. 2954–2979. https://doi.org/10.1080/10407782.2023.2297000.
67. Sahoo, A. & Nandkeolyar, R. (2021). Entropy generation and dissipative heat transfer analysis of mixed convective hydromagnetic flow of a Casson nanofluid with thermal radiation and Hall current. *Scientific Reports*, vol. 11, article 3926. https://doi.org/10.1038/s41598-021-83124-0.
68. Renuka, S., Narender, G., & Govardhan, K. (2024). The effect of a slip wall on radiate magnetohydrodynamic Casson nanofluid past a stretching surface with viscous dissipation: Numerical approach. *Numerical Heat Transfer, Part B: Fundamentals*, vol. 85, iss. 12, pp. 1786–1800. https://doi.org/10.1080/10407790.2023.2274447.
69. Aroloye, S. J., Fenuga, O. J., Abiala, I. O., & Odesola, A. S. (2024). MHD Casson nanofluid flow with viscous dissipation, chemical reaction and thermal radiation subjected to convective boundary conditions. *Unilag Journal of Mathematics and Applications*, vol. 4, no. 1, pp. 8–20.
70. Al-Kouz, W. & Owhaib, W. (2022). Numerical analysis of Casson nanofluid three-dimensional flow over a rotating frame exposed to a prescribed heat flux with viscous heating. *Scientific Reports*, vol. 12, article 4256. https://doi.org/10.1038/s41598-022-08211-2.
71. Syam, M. M., Alkhedher, M., & Syam, M. I. (2025). Thermal and hydrodynamic analysis of MHD nanofluid flow over a permeable stretching surface in porous media: Comparative study of Fe_3O_4, Cu, and Ag nanofluids. *International Journal of Thermofluids*, vol. 26, article 101055. https://doi.org/10.1016/j.ijft.2025.101055.
72. El-ashhab, A. G., Wahab, M. A., Hamza, S. E. E., Moatimid, G. M., & Waheed, S. E. (2025). Effect of nanoparticle aggregation on Casson nanofluid flow at a stagnation point with modified Darcy model and entropy generation. *Discover Applied Sciences*, vol. 7, article 1305. https://doi.org/10.1007/s42452-025-07791-8.
73. Crane, L. J. (1970). Flow past a stretching plate. *Journal of Applied Mathematics and Physics (ZAMP)*, vol. 21, iss. 4, pp. 645–647. https://doi.org/10.1007/BF01587695.

Received 01 June 2026 *Accepted 24 July 2026* *Published 30 September 2026*

Електропровідний потік МГД-нанорідини Кассона в однорідному поперечному магнітному полі над листом, що розтягується

[1] F. T. Onojovwo, [2] A. O. Oyem, [1] S. O. Imoni, [1] J. M. Gyegwe

[1] Федеральний університет Локоджа, P. M. B. 1154, Lokoja, Нігерія

[2] Університет Бусітема, P.O. Box 236, Tororo, Уганда

Це дослідження зосереджене на формулюванні об'ємної відчутної ентальпії нанорідин на основі етиленгліколю, що замінює традиційне температурне рівняння енергії. Нанорідина містить наночастинки Al_2O_3 з об'ємними частками в діапазоні $(0,01\leq\varphi\leq0,05)$, що відповідає експериментально дослідженим концентраціям. На відміну від традиційних температурних формулювань енергії, цей підхід описує перенесення тепла через об'ємну відчутну ентальпію, яка представляє відчутну енергію, збережену на одиницю об'єму нанорідини. Ця структура дозволяє аналізувати зв'язаний рух, ентальпію та перенесення наночастинок в електропровідних нанорідинах Кассона, включаючи термофорез, в'язку дисипацію та джоулеве нагрівання. Рівняння руху, ентальпії та концентрації наночастинок були перетворені на зв'язані нелінійні звичайні диференціальні рівняння за допомогою перетворень подібності та розв'язані чисельно за допомогою адаптивної схеми колокації (SciPy's solve_bvp). Систематично оцінюються ефекти параметрів, включаючи параметр Кассона, параметр магнітного поля, число Шмідта, число Біо, теплове та розчинне числа Грасгофа, число Брінкмана, число Екерта та параметр термофорезу. Результати показують, що параметр магнітного поля та реологічні ефекти Кассона сильно впливають на характеристики руху потоку. Збільшення параметра магнітного поля пригнічує розподіл швидкості через силу Лоренца, одночасно збільшуючи об'ємну відчутну ентальпію завдяки джоулевому нагріванню. Число Екерта призводить до значного збільшення об'ємної відчутної ентальпії завдяки в'язкій дисипації, тоді як число Шмідта переважно контролює перенесення концентрації наночастинок, маючи лише слабкий вплив на поле ентальпії. Теплові та розчинні параметри плавучості посилюють рух рідини завдяки конвекції, зумовленій плавучістю, тоді як термофорез сприяє міграції наночастинок та помірно збільшує накопичення теплової енергії в пограничному шарі. Натомість числа Біо та Брінкмана демонструють обмежений вплив на швидкість, об'ємну відчутну ентальпію та профілі концентрації в межах розглянутих діапазонів параметрів. Запропоноване формулювання об'ємної відчутної ентальпії забезпечує альтернативну основу для кількісної оцінки внутрішнього зберігання та перерозподілу енергії в МГД-неньютонівських нанорідинах. Потенційні застосування включають накопичення теплової енергії, електронне охолодження за допомогою нанорідин, екструзію полімерів, магнітогідродинамічне (МГД) перекачування, біомедичні потоки, збір сонячної теплової енергії та охолодження ядерних реакторів.

***Ключові слова**: об'ємна відчутна ентальпія, формулювання ентальпії, змішана конвекція, МГД, число Брінкмана, перенесення наночастинок.*

Література

1. Okonkwo E. C., Wole-Osho I., Al-Ansari T. An updated review of nanofluids in various heat transfer devices. *Journal of Thermal Analysis and Calorimetry*. 2021. Vol. 145. Iss. 6. P. 2817–2872. https://doi.org/10.1007/s10973-020-09760-2.
2. Kleinstreuer C., Feng Y. Experimental and theoretical studies of nanofluid thermal conductivity enhancement: A review. *Nanoscale Research Letters*. 2011. Vol. 6. Article 229. https://doi.org/10.1186/1556-276X-6-229.
3. Sridhara V., Satapathy L. N. Al_2O_3-based nanofluids: A review. *Nanoscale Research Letters*. 2011. Vol. 6. Article 456. https://doi.org/10.1186/1556-276X-6-456.
4. Hemmat Esfe M., Karimipour A., Yan W.-M., Akbari M., Safaei M. R., Dahari M. Experimental study on thermal conductivity of ethylene glycol based nanofluids containing Al_2O_3 nanoparticles. *International Journal of Heat and Mass Transfer*. 2015. Vol. 88. P. 728–734. https://doi.org/10.1016/j.ijheatmasstransfer.2015.05.010.
5. Xu J., Bandyopadhyay K., Jung D. Experimental investigation on the correlation between nanofluid characteristics and thermal properties of Al_2O_3 nanoparticles dispersed in ethylene glycol–water mixture. *International Journal of Heat and Mass Transfer*. 2016. Vol. 94. P. 262–268. https://doi.org/10.1016/j.ijheatmasstransfer.2015.11.056.
6. Sundar L. S., Ramana E. V., Singh M. K., Sousa A. C. M. Thermal conductivity and viscosity of stabilized ethylene glycol and water mixture Al_2O_3 nanofluids for heat transfer applications: An experimental study. *International Communications in Heat and Mass Transfer*. 2014. Vol. 56. P. 86–95. https://doi.org/10.1016/j.icheatmasstransfer.2014.06.009.

7. Zakaria I., Azmi W. H., Mohamed W. A. N. W., Mamat R., Najafi G. Experimental investigation of thermal conductivity and electrical conductivity of Al_2O_3 nanofluid in water–ethylene glycol mixture for proton exchange membrane fuel cell application. *International Communications in Heat and Mass Transfer*. 2015. Vol. 61. P. 61–68. https://doi.org/10.1016/j.icheatmasstransfer.2014.12.015.
8. Adogbeji V. O., Atofarati E. O., Sharifpur M., Meyer J. P. Magnetohydrodynamics of nanofluid internal forced convection: A review and outlook for practical applications. *Results in Physics*. 2025. Vol. 68. Article 108082. https://doi.org/10.1016/j.rinp.2024.108082.
9. Abd Elfatah M. G., Abd-Ellatif O. E., Attia A. A. A., Elnady A. O. State of art on the role of using a nanofluid in enhancing heat transfer in microchannels with different geometries. *Journal of Engineering and Applied Science*. 2024. Vol. 71. Article 218. https://doi.org/10.1186/s44147-024-00557-w.
10. Sowmiya C., Rushi Kumar B., Bég O. A., Kuharat S. Modeling and analysis of MHD free convective thermo-solutal transport in Casson fluid flow with radiative heat flux. *Journal of Thermal Analysis and Calorimetry*. 2024. Vol. 149. P. 6195–6209. https://doi.org/10.1007/s10973-024-13115-6.
11. Casson N. A flow equation for pigment-oil suspensions of the printing ink type. In: Mill, C. C. (ed.) Rheology of Disperse Systems. London: Pergamon Press, 1959. P 84–104.
12. Khan D., Ali G. Comparative study of dusty tetra hybrid Casson nanofluid flowing in a generalized two-phase MHD medium between parallel microplates with a porous medium. *European Physical Journal Special Topics*. 2024. Vol. 233. P. 2225–2243. https://doi.org/10.1140/epjs/s11734-024-01184-5.
13. Reddy M. V., Vajravelu K., Lakshminarayana P., Sucharitha G. Heat source and Joule heating effects on convective MHD stagnation point flow of Casson nanofluid through a porous medium with chemical reaction. *Numerical Heat Transfer, Part B: Fundamentals*. 2024. Vol. 85. Iss. 3. P. 286–304. https://doi.org/10.1080/10407790.2023.2233694.
14. Khan W., Khan W., Hussain S., Salah B. (A mathematical model of Casson nanofluid flow over a vertically stretched porous surface along with bioconvection, Joule heating and thermal Robin conditions. *Journal of Applied Mathematics and Mechanics*. 2024. Vol. 165. Iss. 9. https://doi.org/10.1177/16878132241275435.
15. Olkha A., Choudhary R. Numerical simulation of MHD radiative Casson nanofluid flow over a nonlinearly heated stretching sheet embedded in porous medium. *Journal of Computational and Theoretical Transport*. 2024. Vol. 53. Iss. 3. P. 184–206. https://doi.org/10.1080/23324309.2024.2332677.
16. Huang J. S., Wang X. W. Analysis of heat and mass transfer in nanofluid flow over a stretching surface in a porous medium considering thermophoretic and Darcy effects. *Boundary Value Problems*. 2026. Vol. 2026. Article 111. https://doi.org/10.1186/s13661-026-02299-5.
17. Talukdar B., Pal D. Induced magnetic field effects on thermophoretic and visco-dissipative chemically reactive thermo-radiative flows. *Thermal Advances*. 2025. Vol. 4. Article 100054. https://doi.org/10.1016/j.thradv.2025.100054.
18. Alao S., Abdulkareem F. A., Ogunmola O. J., Oderinu R. A. Theoretical investigation of heat and mass transfer in unsteady magnetohydrodynamic Williamson nanofluid flow past a permeable stretching surface with viscous dissipation effect. *Thermal Advances*. 2026. Vol. 6. Article 100101. https://doi.org/10.1016/j.thradv.2026.100101.
19. Alrihieli H., Aldhabani M. S. Analysis of dissipative slip flow in couple stress nanofluids over a permeable stretching surface for heat and mass transfer optimization. *Case Studies in Thermal Engineering*. 2025. Vol. 67. Article 105819. https://doi.org/10.1016/j.csite.2025.105819.
20. Yasmin H. Enhanced thermal analysis of bioconvective magnetized Ree–Eyring nanofluid flow on a stretching sheet with Cattaneo–Christov heat flux and microorganism dynamics. *Case Studies in Thermal Engineering*. 2025. Vol. 68. Article 106814. https://doi.org/10.1016/j.csite.2025.106814.
21. Panda S., Shamshuddin M. D., Obalalu A. M., Salawu S. O., Mishra S. R. Cattaneo–Christov hypothesis in a micropolar nanofluid flow over a stretching sheet subjected to exponential space-based heat generation and bilateral reactions. *Case Studies in Thermal Engineering*. 2025. Vol. 68. Article 106813. https://doi.org/10.1016/j.csite.2025.106813.
22. Reddy G. J., Deepthi V. V. L., Raju R. S., Reddy B. M., Ali F. Computational modelling of thermal and mass transport in MHD nanofluid flow across a non-linear surface with chemical response and viscous dissipation. *Modeling Earth Systems and Environment*. 2025. Vol. 11. Article 254. https://doi.org/10.1007/s40808-025-02440-w.
23. Hussain Z., Ayaz M., Islam S., Abualnaja K. M., Sulaiman M. Heat and mass transfer analysis of MHD hybrid nanofluid flow with microorganism over a bi-directional stretching sheet: Effects of thermophoresis and Brownian motion. *International Journal of Dynamics and Control*. 2025. Vol. 8. Article 306. https://doi.org/10.1007/s41939-025-00880-6.
24. Verma D., Mehta R. Numerical investigation of micropolar aluminum oxide nanofluid flow over an inclined stretching sheet. *Discover Applied Sciences*. 2026. Vol. 8. Article 311. https://doi.org/10.1007/s42452-026-08268-y.

25. Reddy G. J., Mangathai P., Pothanna N. Analysis of heat generation impact on nanofluid flow over a stretching sheet. *Partial Differential Equations in Applied Mathematics*. 2024. Vol. 11. Article 10085. https://doi.org/10.1016/j.padiff.2024.100852.
26. Priyadharshini P., Karpagam V., Shah N. A., Alshehri M. H. Bio-convection effects of MHD Williamson fluid flow over a symmetrically stretching sheet: machine learning. *Symmetry*. 2023. Vol. 15. Iss. 9. Article 1684. https://doi.org/10.3390/sym15091684.
27. Sankari M. S., Rao M. E., Awwad F. A., Ismail E. A. A., Makinde O. D., Khan W. Influence of dual stratification on the magnetohydrodynamic flow of Jeffrey nanofluid over an exponentially stretching permeable sheet with viscous dissipation and Joule heating. *Frontiers in Chemistry*. 2025. Vol. 12. Article 1451053. https://doi.org/10.3389/fchem.2024.1451053.
28. Kamath A. V., Puneeth V., Nisar K. S. Modeling and analysis of the bioconvective flow of nanofluid over a stretching sheet with Thompson–Troian slip condition. *Journal of Thermal Analysis and Calorimetry*. 2025. Vol. 150. Iss. 26. P. 14921–14931. https://doi.org/10.1007/s10973-025-14921-2.
29. Preeti, Sharma P., Chaudhary R., Sharma B. K., Govind, Meena R. R. Investigation of Brownian motion/thermophoresis impacts on radiative viscoelastic chemically reactive magnetite fluid flow on a stretching sheet. *Discover Applied Sciences*. 2026. Vol. 8. Article 608. https://doi.org/10.1007/s42452-026-08596-z.
30. Khader M. M., Adel M., Babatin M. M., Alaidrous A. Williamson nanofluid flow and thermal transfer generated by a convectively heated stretched sheet via Fibonacci–Luca's polynomials. *AIMS Mathematics*. 2025. Vol. 10. Iss. 12. P. 29012–29036. https://doi.org/10.3934/math.20251276.
31. Khalila K. M., Mohammed F. A., Abbas W., Megahed A. M. Exploring slip boundary impacts on magnetohydrodynamic Casson nanofluid flow over a vertical stretching sheet with nonlinear thermal radiation. *Journal of Taibah University for Science*. 2025. Vol. 19. Iss. 1. https://doi.org/10.1080/16583655.2025.2565855.
32. Sankari M. S., Rao M. E., Shams Z. E., Algarni S., Sharif M. N., Alqahtani T., Eid M. R., Jamshed W., Irshad K. Williamson MHD nanofluid flow via a porous exponentially stretching sheet with bioconvective fluxes. *Case Studies in Thermal Engineering*. 2024. Vol. 59. Article 104453. https://doi.org/10.1016/j.csite.2024.104453.
33. Liu Q., He Y.-L., Li Q. Enthalpy-based multiple-relaxation-time lattice Boltzmann method for solid-liquid phase-change heat transfer in metal foams. *Physical Review E*. 2017. Vol. 96. Iss. 2. Article 023303. https://doi.org/10.1103/PhysRevE.96.023303.
34. Ramakrishnan T., Bhalla A. P. S. A low Mach enthalpy method to model non-isothermal gas–liquid–solid flows with melting and solidification. *International Journal of Multiphase Flow*. 2023. Vol. 169. Article 104605. https://doi.org/10.1016/j.ijmultiphaseflow.2023.104605.
35. Santos A. C., Sacomano Filho F. L., Vié A. The general formulation of the energy equation and the impact of enthalpy diffusion on multi-component droplet heat and mass transfer. *International Journal of Heat and Mass Transfer*. 2023. Vol. 210. Article 124172. https://doi.org/10.1016/j.ijheatmasstransfer.2023.124172.
36. Elbashbeshy E. M. A., Ibrahim F. N. Steady free convection flow with variable viscosity and thermal diffusivity along a vertical plate. *Journal of Physics D: Applied Physics*. 1993. Vol. 26. Iss. 12. Article 2137. https://doi.org/10.1088/0022-3727/26/12/007.
37. Seddeek M. A., Abdelmeguid M. S. The effects of radiation and thermal diffusivity on heat transfer over stretching surface with variable heat flux. *Physics Letters A*. 2006. Vol. 348. Iss. 3–6. P. 172–179. https://doi.org/10.1016/j.physleta.2005.01.101.
38. Xuan Y., Roetzel W. Conceptions for heat transfer correlation of nanofluids. *International Journal of Heat and Mass Transfer*. 2000. Vol. 43. Iss. 19. P. 3701–3707. https://doi.org/10.1016/S0017-9310(99)00369-5.
39. Pak P. C., Cho Y. I. Magnetohydrodynamic and heat transfer of dispersed fluids with submicron metallic oxide particles and experimental heat transfer. *Journal of Thermal Energy Generation, Transport, Storage, and Conversion*. 1998. Vol. 11. Iss. 2. P. 151–170. https://doi.org/10.1080/08916159808946559.
40. Maiga S. E. B., Nguyen C. T., Galanis N., Roy G. Heat transfer behaviours of nanofluids in a uniformly heated tube. *Superlattices and Microstructures*. 2004. Vol. 35. Iss. 3–6. P. 543–557. https://doi.org/10.1016/j.spmi.2003.09.012.
41. Asogwa K. K., Ibe A. A. A study of MHD Casson fluid flow over a permeable stretching sheet with heat and mass transfer. *Journal of Engineering Research and Reports*. 2020. Vol. 16. Iss. 2. P. 10–25. https://doi.org/10.9734/JERR/2020/v16i217161.
42. Kasali K. B., Gbadamosi B., Familua A. B., Tairu M. L. Heat and mass transfer of an MHD Casson fluid with variable properties and non-linear thermal radiation over an elastic sheet. *Journal of Applied and Physical Sciences*. 2024. Vol. 2. No. 1. P. 80–87.
43. Das U. J. MHD boundary layer flow of Casson fluid past an inclined plate in the presence of Soret / Dufour effects, heat source and first-order chemical reaction. *Journal of Scientific Research*. 2021. Vol. 13. No. 3. P. 785–795. https://doi.org/10.3329/jsr.v13i3.52234.

44. Puneeth V., Manjunatha S., Madhukesh J. K., Ramesh G. K. Three-dimensional mixed convection flow of hybrid Casson nanofluid past a non-linear stretching surface: a modified Buongiorno's model aspects. *Chaos, Solitons and Fractals*. 2021. Vol. 152. Article 111428. https://doi.org/10.1016/j.chaos.2021.111428.
45. Abbas N., Shatanawi W., Hasan F., Shatnawi T. A. M. Investigation of MHD radiative Casson micropolar hybrid nanofluid over exponential curved stretching sheet. *Journal of Radiation Research and Applied Sciences*. 2024. Vol. 18. Iss. 1. Article 101269. https://doi.org/10.1016/j.jrras.2024.101269.
46. Kumar V. V., Raja Shekar M. N. Heat and mass transfer in radiative MHD Casson nanofluid flow over a nonlinear stretching sheet. *International Journal of Applied Mathematics*. 2024. Vol. 37. No. 6S. Article 1893. https://doi.org/10.12732/ijam.v37i6s.1893.
47. Manthramurthy P., Vempati S. R. Significance of multiple slips and thermal radiation on heat and mass transfer in MHD Casson nanofluid flow over an exponentially stretching porous sheet with non-uniform heat source and sink. *Multiscale and Multidisciplinary Modeling, Experiments and Design*. 2025. Vol. 8. Article 157. https://doi.org/10.1007/s41939-025-00743-0.
48. Vinutha K., Madhukesh J. K., Prasad K. V., Kulshreshta A., Shah N. A., Yar M. MHD Casson nanofluid flow over a three-dimensional exponentially stretching surface with waste discharge concentration: A revised Buongiorno's model. *Applied Rheology*. 2025. Vol. 35. No. 1. P. 20250040. https://doi.org/10.1515/arh-2025-0040.
49. Algehyne E. A., Yasmin H., Alduais F. S., Al-Bossly A., Khan A. Thermal analysis of Cattaneo–Christov heat/mass flux model effects on radiative Casson nanofluid flow past a bi-directional extending sheet subject to exponential heat source with machine learning approach. *Open Physics*. 2026. Vol. 24. No. 1. P. 20250254. https://doi.org/10.1515/phys-2025-0254.
50. Prakash O. Dissipative stagnation point flow of the Casson nanofluid over a stretching sheet under the influence of porous media, binary chemical reaction and variable surface heat flux condition. *Pramana – Journal of Physics*. 2025. Vol. 99. Article 31. https://doi.org/10.1007/s12043-024-02873-5.
51. Aroloye S. J., Fenuga O. J., Abiala I. O. Analysis of radiative hydromagnetic Casson nanofluid flow with convective boundary condition. *Ife Journal of Science*. 2025. Vol. 27. No. 1. https://doi.org/10.4314/ijs.v27i1.2s.
52. Khan A., Hashim, Farooq M., Hussain S.M., Ahmad H., Jamshed W., Eid M. R., Abdalla N. S. E. Heat and mass transfer in magnetic Casson nanofluids flow with radiation and stratification effects: Thermal management applications. *Journal of Radiation Research and Applied Sciences*. 2025. Vol. 18. Iss. 4. Article 102019. https://doi.org/10.1016/j.jrras.2025.102019.
53. Vinodkumar Reddy M., Lakshminarayana P., Vajravelu K., Sucharitha G. Activation of energy in MHD Casson nanofluid flow through a porous medium in the presence of convective boundary conditions and suction/injection. *Numerical Heat Transfer Part A: Applications*. 2025. Vol. 86. Iss. 5. P. 1069–1085. https://doi.org/10.1080/10407782.2023.2271655.
54. Priyadharshini P., Sowndharya M., Chamkha A. J. Thermal and flow analysis of chemically reactive Casson hybrid nanofluids with machine learning validation. *Mechanics of Time-Dependent Materials*. 2025. Vol. 29. Article 74. https://doi.org/10.1007/s11043-025-09812-w.
55. Duguma K. A. Effects of buoyancy on radiative MHD mixed convective flow of Casson nanofluid across a preamble slippery sheet in Darcy-Forchheimer porous medium: Shrinking/stretching surface mode. *Numerical Heat Transfer, Part B: Fundamentals*. 2026. Vol. 87. Iss. 1. https://doi.org/10.1080/10407790.2025.2532116.
56. Saleem M., Al-Zubaidi A., Tufail M. N., Fiaz Z., Saleem S. Exploration of numerical simulation for unsteady Casson nanofluid thin film flow over stretching surface with mixed convection effects using Buongiorno's nanofluid model. *ZAMM – Zeitschrift für Angewandte Mathematik und Mechanik*. 2024. Vol. 104. Iss. 12. Article e202400165. https://doi.org/10.1002/zamm.202400165.
57. Javid K., Akbar N. S., Shaiq S., Khan A., Jamshed W., Hussain S. M., Guedri K., Ahmad H., Abd-Elmonem A. MHD Casson nanofluid flow over a vertical stretchable sheet saturated with a porous medium: A parametric approach for sensitive analysis. *Discover Nano*. 2026. Vol. 21. Article 209. https://doi.org/10.1186/s11671-026-04667-7.
58. Seada M. M., Saeed A. Thermal analysis of Casson hybrid nanofluid flow with solar radiation and inclined magnetic field. *Chemical Engineering and Technology*. 2026. Vol. 49. Iss. 3. Article e70203. https://doi.org/10.1002/ceat.70203.
59. Samaila G., Jha B. K. Heat and mass transfer mixed convection Casson MHD nanofluid flow over a vertical plate with nonlinear thermal radiation. *SSRN*, 2025. 32 p. https://doi.org/10.2139/ssrn.5391612.
60. Ajithkumar M. Thermo-solutal dynamics of electroactive Casson nanofluid flow through an uneven asymmetric conduit for advanced microfluidic applications. *Advanced Theory and Simulations*. 2025. Vol. 8. No. 12. Article e01148. https://doi.org/10.1002/adts.202501148.
61. Akolade M. T., Idowu A. S. Radiation effect on gravity-driven nanofluid flow over a convective heated wall: RSM and ANN prediction analysis. *Nano-Structures and Nano-Objects*. 2025. Vol. 43. Article 101506. https://doi.org/10.1016/j.nanoso.2025.101506.

62. Enyadene L. G., Rikitu E. H., Gabissa A. F. Numerical investigation of heat and mass transfer of variable viscosity Casson nanofluid flow through a microchannel filled with a porous medium. *Journal of Applied Math*. 2023. Vol. 1. No. 3. Article 194. https://doi.org/10.59400/jam.v1i3.194.
63. Kumar J., Chand K., Thakur P. Numerical study of hall current and thermophoresis effect on the hydromagnetic Casson nanofluid flow over a stretching surface. *Journal of the Nigerian Society of Physical Sciences*. 2026. Vol. 8. Iss. 2. Article 3259. https://doi.org/10.46481/jnsps.2026.3259.
64. Khan S., Kumar D., Kumar R., Mehta R. Study of unsteady Casson nanofluid flow across a stretching surface embedded in a porous medium in the presence of Stefan blowing and radiation. *Journal of Thermal Analysis and Calorimetry*. 2025. Vol. 150. P. 22363–22373. https://doi.org/10.1007/s10973-025-14778-5.
65. Tawade J. V., Guled C. N., Noeiaghdam S., Fernandez-Gamiz U., Govindan V., Balamuralitharan S. Effects of thermophoresis and Brownian motion for thermal and chemically reacting Casson nanofluid flow over a linearly stretching sheet. *Results in Engineering*. 2022. Vol. 15. Article 100448. https://doi.org/10.1016/j.rineng.2022.100448.
66. Paul A., Sarma N., Patgiri B. Thermal and mass transfer analysis of Casson-Maxwell hybrid nanofluids through an unsteady horizontal cylinder with variable thermal conductivity and Arrhenius activation energy. *Numerical Heat Transfer Part A: Applications*. 2025. Vol. 86. Iss. 9. P. 2954–2979. https://doi.org/10.1080/10407782.2023.2297000.
67. Sahoo A., Nandkeolyar R. Entropy generation and dissipative heat transfer analysis of mixed convective hydromagnetic flow of a Casson nanofluid with thermal radiation and Hall current. *Scientific Reports*. 2021. Vol. 11. Article 3926. https://doi.org/10.1038/s41598-021-83124-0.
68. Renuka S., Narender G., Govardhan K. The effect of a slip wall on radiate magnetohydrodynamic Casson nanofluid past a stretching surface with viscous dissipation: Numerical approach. *Numerical Heat Transfer, Part B: Fundamentals*. 2024. Vol. 85. Iss. 12. P. 1786–1800. https://doi.org/10.1080/10407790.2023.2274447.
69. Aroloye S. J., Fenuga O. J., Abiala I. O., Odesola A. S. MHD Casson nanofluid flow with viscous dissipation, chemical reaction and thermal radiation subjected to convective boundary conditions. *Unilag Journal of Mathematics and Applications*. 2024. Vol. 4. No. 1. P. 8–20.
70. Al-Kouz W., Owhaib W. Numerical analysis of Casson nanofluid three-dimensional flow over a rotating frame exposed to a prescribed heat flux with viscous heating. *Scientific Reports*. 2022. Vol. 12. Article 4256. https://doi.org/10.1038/s41598-022-08211-2.
71. Syam M. M., Alkhedher M., Syam M. I. Thermal and hydrodynamic analysis of MHD nanofluid flow over a permeable stretching surface in porous media: Comparative study of Fe_3O_4, Cu, and Ag nanofluids. *International Journal of Thermofluids*. 2025. Vol. 26. Article 101055. https://doi.org/10.1016/j.ijft.2025.101055.
72. El-ashhab A. G., Wahab M. A., Hamza S. E. E., Moatimid G. M., Waheed S. E. Effect of nanoparticle aggregation on Casson nanofluid flow at a stagnation point with modified Darcy model and entropy generation. *Discover Applied Sciences*. 2025. Vol. 7. Article 1305. https://doi.org/10.1007/s42452-025-07791-8.
73. Crane L. J. Flow past a stretching plate. *Journal of Applied Mathematics and Physics (ZAMP)*. 1970. Vol. 21. Iss. 4. P. 645–647. https://doi.org/10.1007/BF01587695.